N72-25335

Oceanographic Scanner System Design Study

Volume II
BSR 3129
October 1971
Ann Arbor, Michigan

Bendix Aerospace Systems Division

Oceanographic Scanner System Design Study

Volume II
BSR 3129
October 1971
Ann Arbor, Michigan

Submitted to:
NASA Headquarters
Washington, D.C.

In Response to:
Contract NASW-2119

Bendix Aerospace Systems Division

CONTENTS

ILLUSTRATIONS

SECTION 1

INTRODUCTION

In conjunction with Contract NASW-2119, to conduct a design of an oceanographic multispectral scanning system, Bendix has sponsored the breadboarding of the scanner collection optics and two channels of electronics. In addition, the scan mechanism has been breadboarded under a contract change, which deleted the requirement to supply hardware development plans and substituted some breadboarding activities in their place. The contract change also required that techniques to increase the duty cycle to above 50% should be investigated.

The complete design of the scanner is reported in Volume I of the final report while the following sections of Volume II cover the activities referred to above. Section 2 briefly describes the optical breadboard, and the results show that adequate optical resolution can be achieved many resolution elements off axis. The sensitivity of the rotor arm to misalignments has also been investigated and verifies the analysis given in Volume I. Section 3 covers the performance of the scan mechanism, giving measurements of both cell-to-cell registration errors and line-to-line underlap/overlap. The former is about 9% of one instantaneous field of view (IFOV) element, while the latter is under 5% of one IFOV element. These measurements show that the motion of the scan mechanism can be controlled to meet the requirements of the scanner. Section 4 covers the electronics breadboard and its performance; Section 5 is devoted to techniques of increasing the duty cycle. In Section 5, various alternative configurations are discussed, and the alignment tolerances are analyzed. The technique selected requires an adjustable rotor arm, which has also been breadboarded to verify whether or not the alignment tolerances can be met. This aspect of the breadboard is in progress and is therefore not discussed further in this report.

SECTION 2

OPTICS BREADBOARD

2.1 RESOLUTION TEST AND DEFOCUSING MEASUREMENT

Although a thorough theoretical analysis of the OSS collecting optics has been made (see Vol 1, Section 3), the addition of a breadboard test is considered to be very advisable since this type of telescope, consisting of a spherical primary and hyperbolic secondary, is practically unknown. The test objectives are, first, to demonstrate that the required resolution of 0.066 milliradian (mrad) can be achieved for all detector positions, and, second, to investigate the sensitivity of the telescope to changes in the primary-to-secondary mirror separation. This separation is the part of the system most sensitive to misalignment and is therefore indicative of the tightest alignment tolerances which have to be held.

In the breadboard, the two mirrors are essentially mounted like a Gregorian telescope as shown in the layout, Figure 2-1. The geometrical data are:

Focal length of the primary:	20.00 in. (508.0 mm)
Diameter of the incident beam:	11.00 in. (279.4 mm)
Focal length of the secondary:	3.57 in. (90.7 mm)
Back focal distance:	12.50 in. (317.5 mm)
Mirror separation:	25.00 in. (635.0 mm)

The image of a test target, a grid with 0.1-mm spacings placed in the focal plane of an 11-in. collimator, is viewed in the focal plane of the telescope. Since the focal length of the collimator is 60.0 in. (1524 mm), the angle corresponding to the grid spacing is:

$$\alpha = \frac{0.1}{1524} \text{ rad} = 0.066 \text{ mrad}$$

Each square in the grid is therefore equivalent to one resolution element or instanteneous field of view (IFOV).

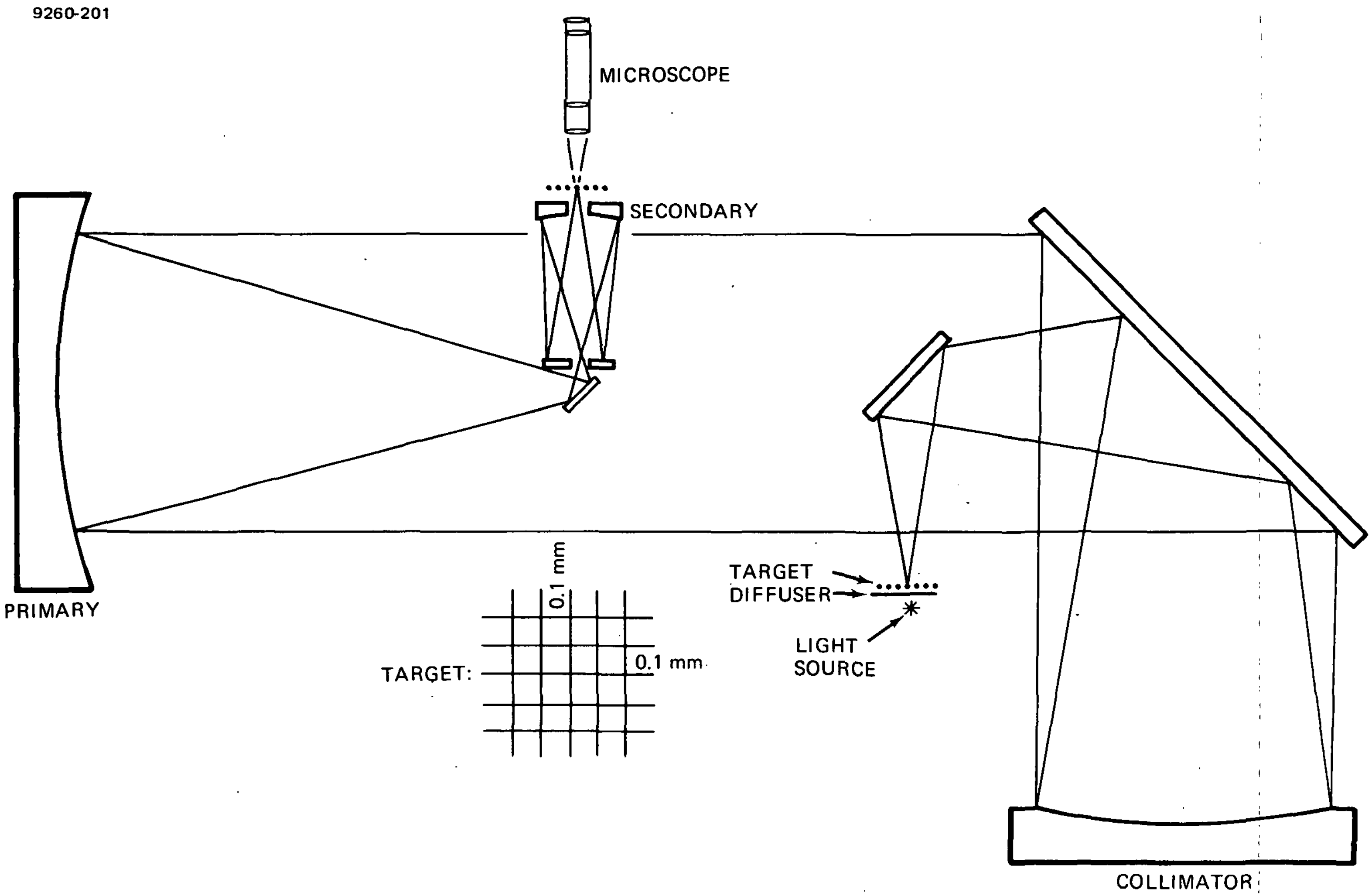

Figure 2-1 Optical Schematic of the Breadboard Optics

Figure 2-2 comprises a series of photographs which show both the image of the grid in the focal plane of the telescope and the effect on the focusing caused by varying the mirror separation in steps of 0.1 mm. The photographs show that the telescope performance is satisfactory many resolution elements off-axis, while the allowed variation in mirror separation is very encouraging with respect to alignment tolerances.

2.2 ROTOR SENSITIVITY TO MISALIGNMENT

The second subject of the test program was the scanning rotor and the optical effect of its misalignment. Again, the most sensitive one of all possible misalignments was chosen for measurement. This can be described as a rotation of the rotor about an axis perpendicular to the axis of rotation and perpendicular to the connection line between the two scan mirrors (see Vol 1, Section 3.6). A layout of the test setup is sketched in Figure 2-3. In this setup, the plane folding mirror between the primary and the rotor is used only for convenience, and the pair of mirrors which comprise the rotor are mounted on a precision rotary table. According to the theoretical treatment of this case, this misalignment results in a line-to-line scan inaccuracy. The linear displacement Δx in the focal plane of the primary which corresponds to a rotational misalignment α is:

$$\Delta x = S \cdot \alpha$$

where S is the separation of the two scan mirrors. This can also be written as:

$$F \cdot \Delta\phi = S \cdot \alpha$$

where F is the focal length of the primary and $\Delta\phi$ is the angular variation in the line of sight resulting from the rotation α.

Using the geometric data of the breadboarded componenets, F = 508 mm and S = 54 mm, a rotatory misalignment of $\alpha = 1' = 2.91 \cdot 10^{-4}$ rad theoretically results in:

$$\Delta\phi = \frac{S \cdot \alpha}{F} = 3.1 \cdot 10^{-5} \text{ rad}$$

The measurement showed that a rotation of the rotor about an angle of 7' resulted in the image in the focal plane of the telescope shifting three elements of resolution. Since one element of resolution corresponds to an angle of 0.066 mrad, we find an angular variation in the line of sight of $\Delta\phi = 2.96 \cdot 10^{-5}$ rad per 1' of rotation, which is in good agreement with the computed amount.

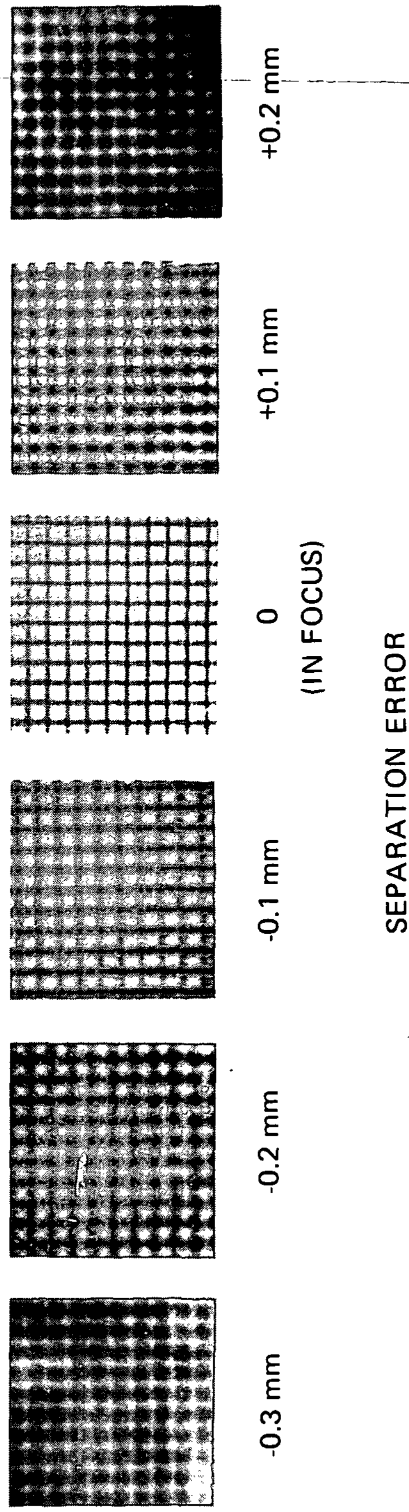

Figure 2-2 Photographs of the Grid for Different Primary to Secondary Separations

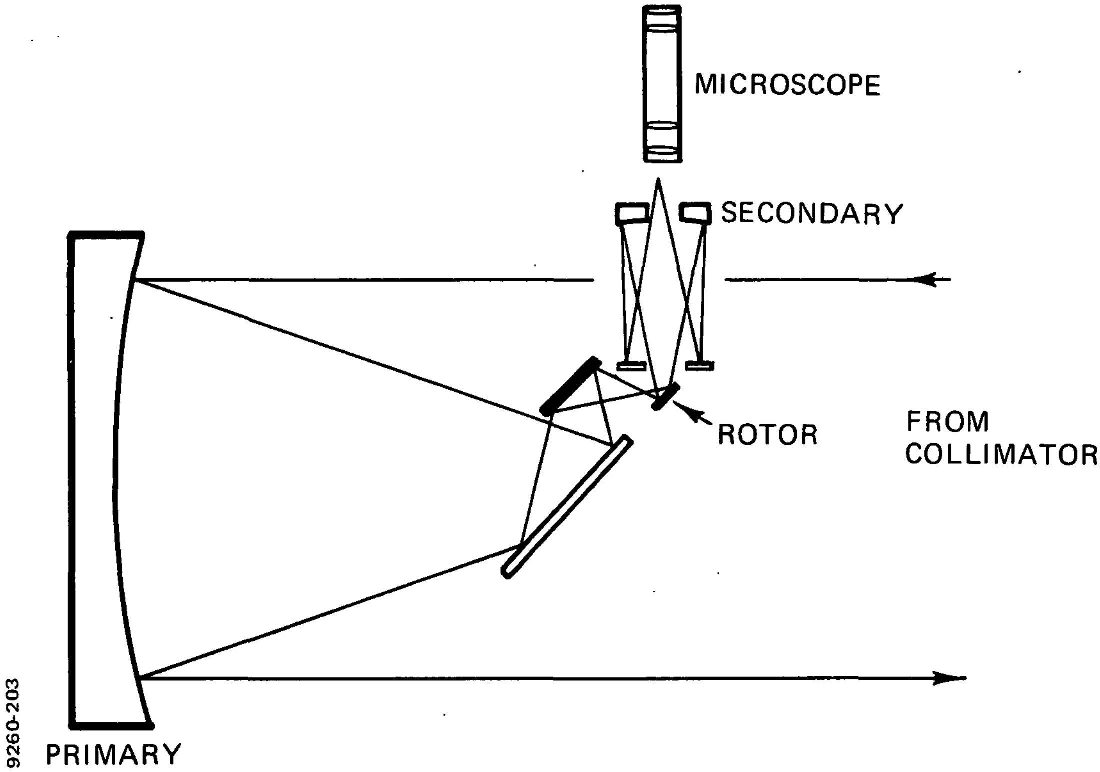

Figure 2-3 Optical Schematic of the Rotor Misalignment Test

SECTION 3

SCAN MECHANISM REGISTRATION TESTS

Measurements of spatial registration errors have been made on a breadboard model of the scan mechanisms and are discussed in the following sections. The breadboard is as representative of a flight unit as is reasonable without going to a space-qualified motor, and very high precision encoder and bearings. The differences between the breadboard and a flight unit are discussed in Section 3.1 from which it is seen that higher precision should be achievable on a flight unit. Section 3.2 then covers the test procedures and Section 3.3 covers the test results. Measurements of both cell-to-cell registration on adjacent scan lines and line-to-line underlap/overlap show that the spatial registration errors are less than 10% of one IFOV. This corresponds to 11 arc-sec (53 μrad) of rotation of the motor shaft or 1.4 arc-sec (6.6 μrad) pointing repeatability in object space.

3.1 BREADBOARD MOTOR, MOTOR CONTROL, AND ROTOR

3.1.1 Motor

A brushless dc motor has been chosen for use on the OSS Scanner. The rationale for this selection is presented in detail in Section 4.5.1 of Vol 1 of this Final Report. The motor used on the breadboard is a dc motor, but a more conventional brush type.

In a conventional dc motor, such as that used on the breadboard, preformed windings are inserted into slots. These slots create a variable reluctance path for the field flux as a function of rotor position. Slotting and commutation effects, then, produce relatively large ripple torques. In comparison, the motor which would be used on the space version of the OSS Scanner employs a constant reluctance magnetic circuit and a precision toroidally distributed coil winding. Consequently, no undesirable slot ripple or varying torque effects vs. motor rotation would be experienced. Therefore, the positional accuracy achievable with the space scanner motor would be superior to that which has been demonstrated with the breadboard model.

The torque output of the motor required to turn the rotor assembly in air has been determined to be less than 2 oz-in. The breadboard motor is rated at 15 oz-in., continuous duty—somewhat higher than the rating of the actual scanner. This variation would, however, have little effect on the achievable positional accuracy.

3.1.2 Motor Control and Encoder

The motor speed control system which would be used on the OSS Scanner is discussed in Section 4.5.1 of Vol 1. The control system used on the breadboard unit is basically the same design utilizing hybrid digital/analog servo techniques. A block diagram is shown in Figure 3-1.

There are, however, two major differences between the encoder used in the breadboard system and that which would be used on the actual scanner. First, the encoder which would be used on the OSS Scanner would have at least 6000 lines, more than three times the number on the breadboard version, which has only 1800 lines. This increase would provide much greater positional accuracy than that which can be achieved with the breadboard unit.

Secondly, the encoder used on the actual scanner would be more accurate than that which is incorporated in the breadboard unit. The disc itself would be more accurate, and an additional readout station would be provided, thereby eliminating the error due to improper centering of the disc. Obviously, the positional accuracy of the over-all scanner system is directly dependent on the encoder accuracy.

A further increase in positional accuracy of the actual scanner will be accomplished through the optimization of the analog motor stabilization circuitry. Minor modification of this circuitry on the breadboard unit was found to be necessary, when the rotor was mounted on the shaft, to account for the increased inertia. Major redesign of this circuitry on the actual scanner will result in the greatest possible accuracy, taking into account the mechanical resonances of the structure as well as the rotor inertia.

3.1.3 Bearings

A rather sophisticated bearing configuration will be used on the OSS Scanner (see Section 4.3 of Vol 1). Three sets of ABEC class 9 angular contact bearings will be used, with a separation of 3.0 in. between the single and duplex sets. The breadboard unit, on the other hand, incorporates two ABEC class 7 bearings, with a separation of 2.5 in. Clearly, misregistration due to bearing runout will be less on the actual scanner than that which is observed in the breadboard testing program.

3.1.4 Rotor

The rotor used on the breadboard version of the scanner is representative of the actual rotor assembly in terms of radius, weight, inertia, and cross-sectional area (for windage effects). There is, however, a major difference in the optical

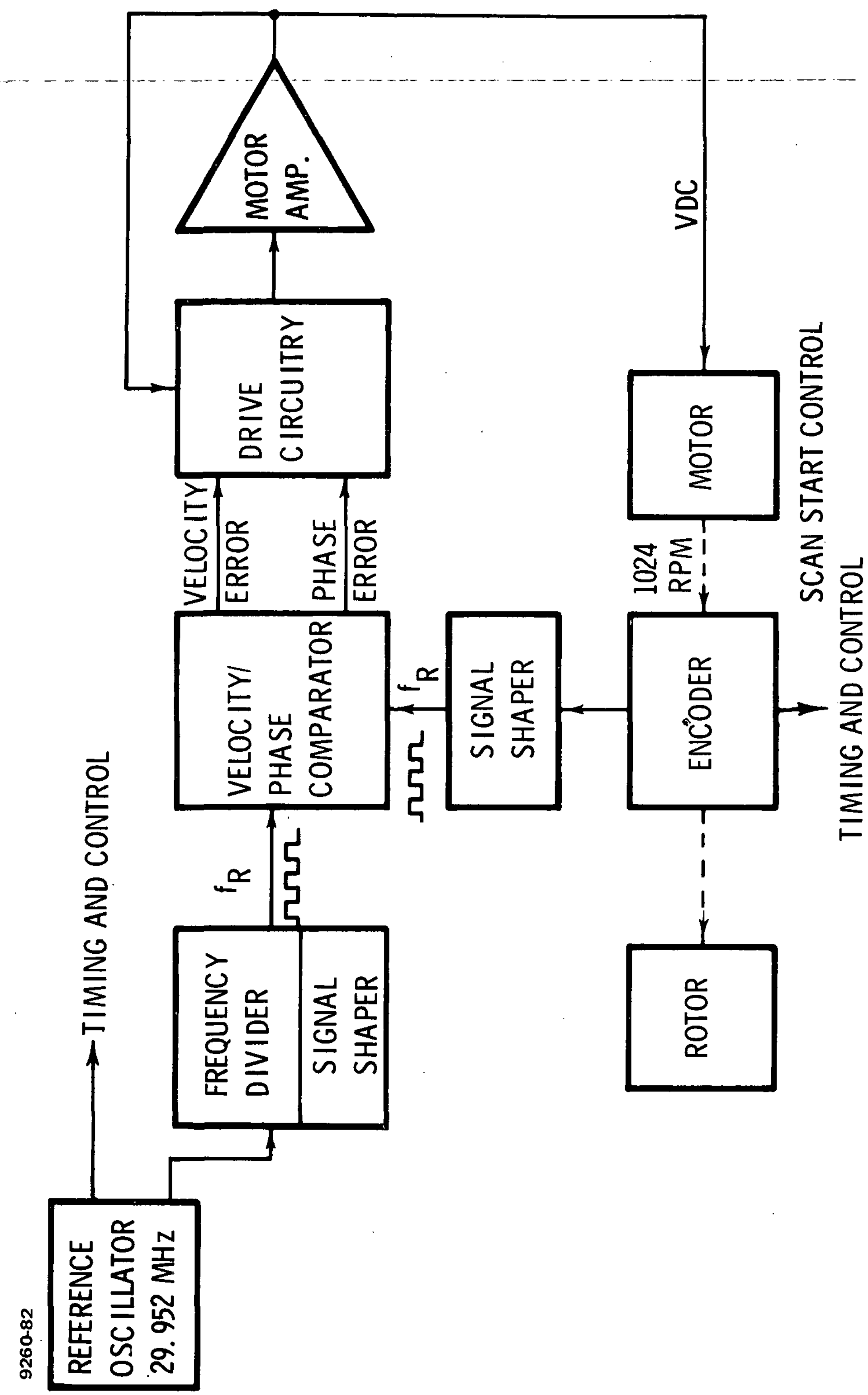

Figure 3-1 Typical DC Motor-Encoder System and Control

design of the two. For convenience in testing, the test rotor acts as a retro-reflector and, apart from a lateral shift, approximately returns an incident ray back along its direction of incidence, as shown in Figure 3.2. The actual rotor will simply shift the ray laterally, but will allow it to continue in approximately the same direction, as shown in Figure 3-3.

As a result of this difference in design, optical registration test data will be conservative. That is, misregistration on the actual scanner caused by lateral movement of thr rotor arm will be negligible, whereas the same lateral movement of the breadboard rotor arm (due to bearing runout) will result in a relatively large registration error.

3.2 TEST PROCEDURES AND APPARATUS

3.2.1 Cell-to-Cell Tests

Measurement of cell-to-cell registration on adjacent scan lines is made in two ways: (1) electronically through the use of the encoder output pulse train and (2) optically through the use of the rotor assembly combined with a light source, target, and detector.

For the electronic test, the system test output of the breadboard motor is used. That signal is a pulse train, Figure 3-4, comprised of the leading edge of the reference pulses and the trailing edge of the encoder pulses. Since there are 1800 lines on the encoder, means is provided to observe only one pulse per revolution of the shaft, the same pulse each time, by counting down the signal by 1800. Variations of the width W of this pulse can be observed on an oscilloscope (see Section 3.3) or measured with a high-speed counter. These variations give a direct measurement of speed fluctuations which lead to cell-to-cell registration errors in adjacent scan lines. The electronic tests can be performed both with and without the rotor attached, giving an indication of the effects of windage on positional accuracy as well as the validity of the motor stabilization circuitry used. It should be noted that electronic tests do not provide any evidence of bearing runout, making optical tests necessary.

In the optical test arrangement, Figure 3-5, a target is imaged, through the rotor arm and a lens, onto a slit. The detector output is a single pulse for each revolution of the rotor arm when a radial slit target is used. A single reference pulse for each revolution of the rotor is obtained by counting down the motor reference pulse train by 1800. The variation in time interval between this reference pulse and the pulse output of the detector gives a direct measurement of cell-to-cell registration in adjacent scan lines, and can be observed either on an oscilloscope or with a high-speed counter. The similarity between the data obtained with

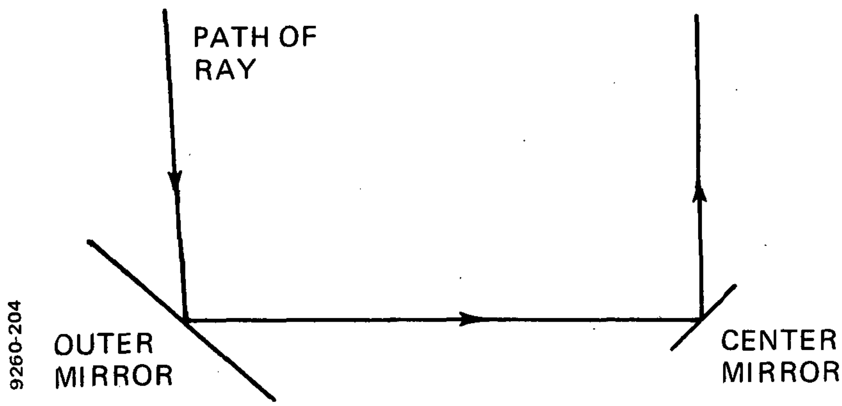

Figure 3-2 Test Rotor

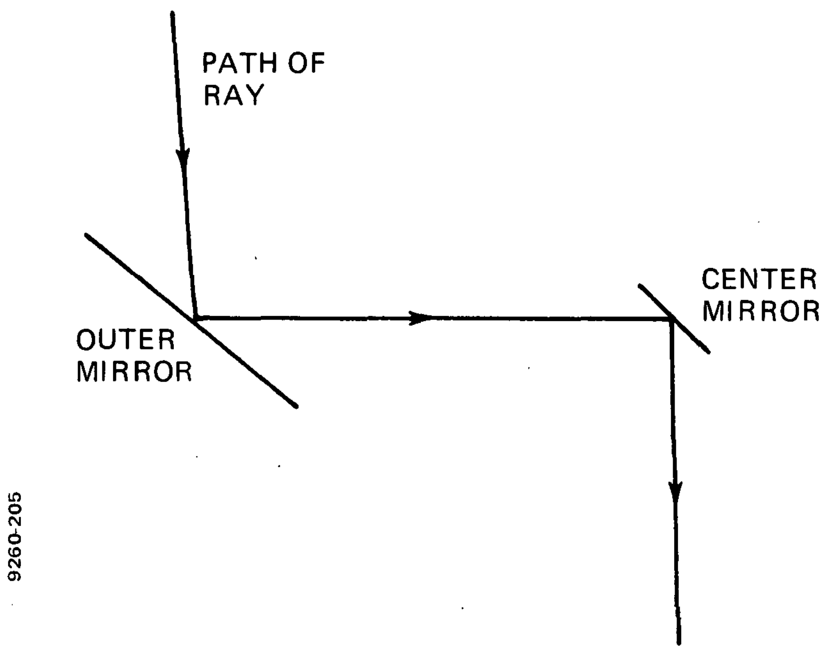

Figure 3-3 Actual Rotor

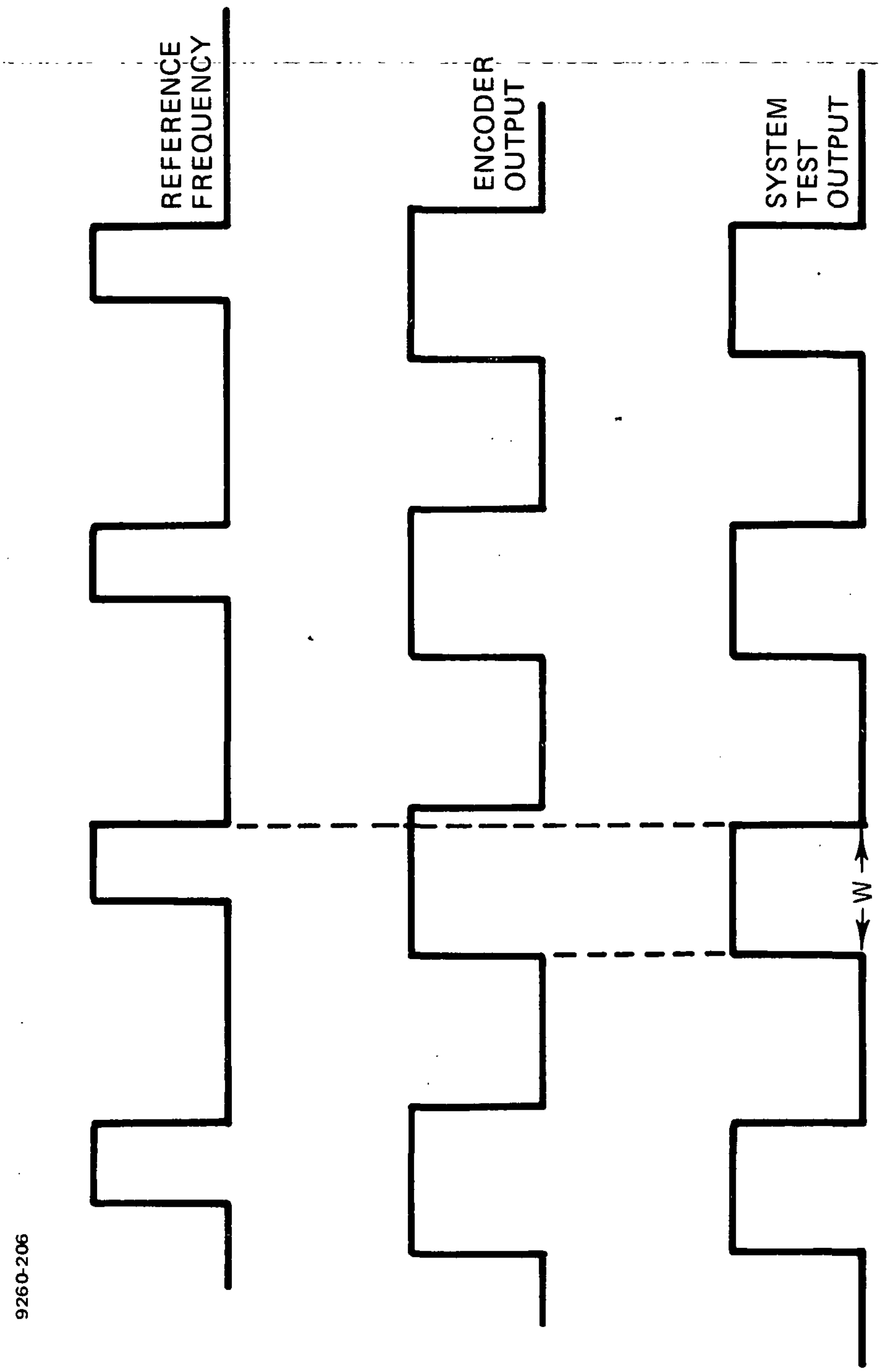

Figure 3-4 System Test Signal Available From the Motor

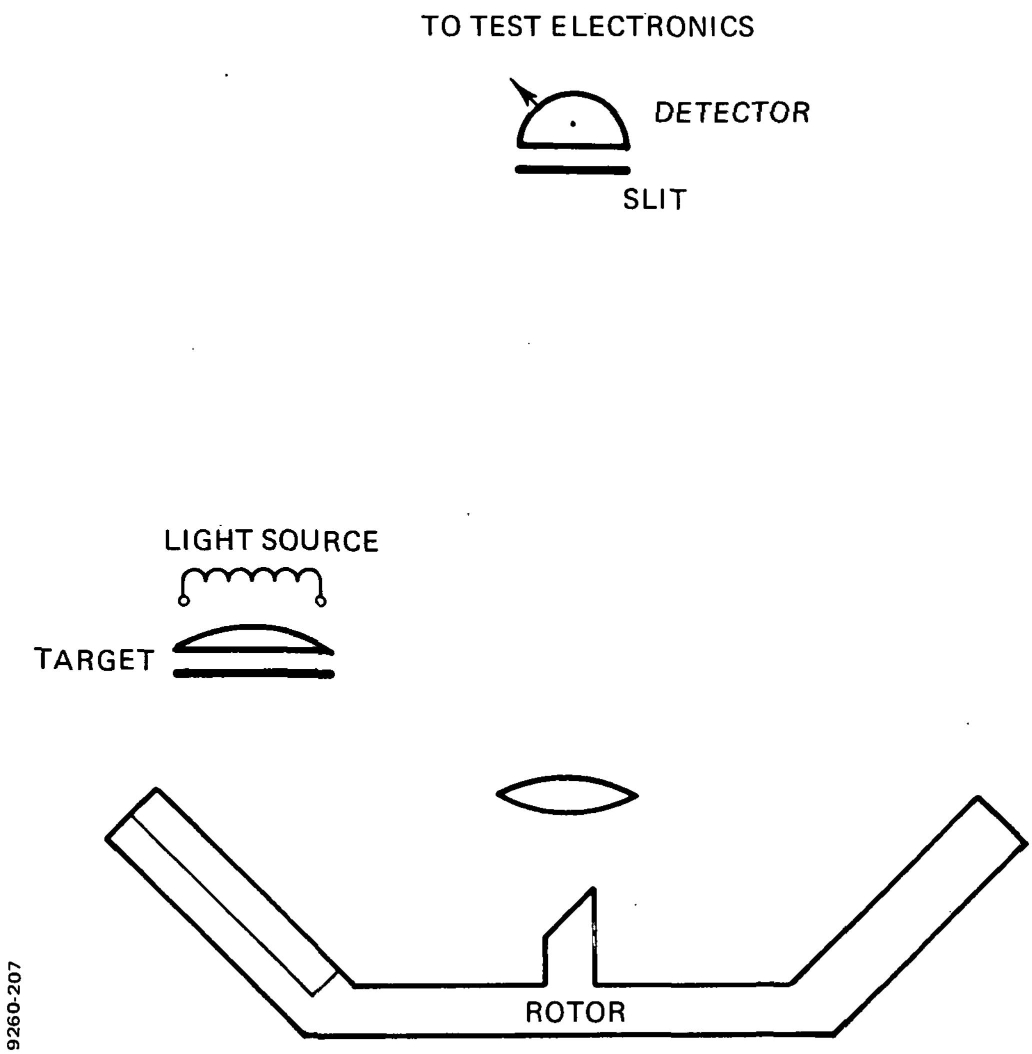

Figure 3-5 Optical Test Arrangement

the electronic (encoder) tests and the optical tests is obvious. The optical tests, however, include the effects of bearing runout on cell-to-cell misregistration.

In the optical tests, it is evident that the reference pulse may occur in any position of the circle scanned by the rotor, Figure 3-6(a), depending on the starting conditions of the motor. A programmable counter is therefore provided which will delay the reference pulse by M clock pulses. The interval M can be adjusted to provide an appropriately short interval τ between the reference pulse and slit pulse so that it may be displayed on an oscilloscope. This interval can also be used to observe different pulses for the electronic encoder test measurements. The test jig is also constructed so that the target assembly may be rotated manually, enabling different parts of a scan to be observed.

3.2.2 Line-to-Line Tests

Line-to-line registration (overlap/underlap) is dependent on two completely independent effects: (1) velocity variations of the motor relative to the nominal speed and (2) bearing errors. The first is measured as part of the cell-to-cell tests, but it should have a completely negligible effect on line-to-line underlap/overlap. The second is measured optically by a test procedure which is similar to that used for cell-to-cell registration tests. Thus, the radial slit is curtailed with a tangential edge driven by a micrometer screw, Figure 3-6(b). The resulting signal from the detector is one pulse per revolution whose height is proportional to the scan line position. Changes in this level from scan-to-scan provide a measure of line-to-line underlap/overlap errors arising from bearing runout. The system can be calibrated by using the micrometer screw to adjust the position of the edge, and many pulses can be conveniently displayed on an oscilloscope by generating a slow sweep.

3.3 TEST RESULTS

3.3.1 Motor Unloaded

Initial testing of the motor/speed control system (without the scan rotor arm attached to the motor shaft) indicated that very good positional accuracy is possible with the chosen system. The motor is driven by a pulse train obtained from the system crystal oscillator (see Figure 3-1). The encoder provides a feedback signal consisting of pulses of the same frequency as the reference (once frequency lock is achieved). A system test signal is available which is a pulse train of the same frequency as the reference. The leading edge of each pulse is the leading edge of a pulse of the driving train. The trailing edge of each pulse is the trailing edge of the corresponding encoder feedback pulse. Figure 3-7(a) is a photograph of this pulse as seen on the face of an oscilloscope. The scope triggers

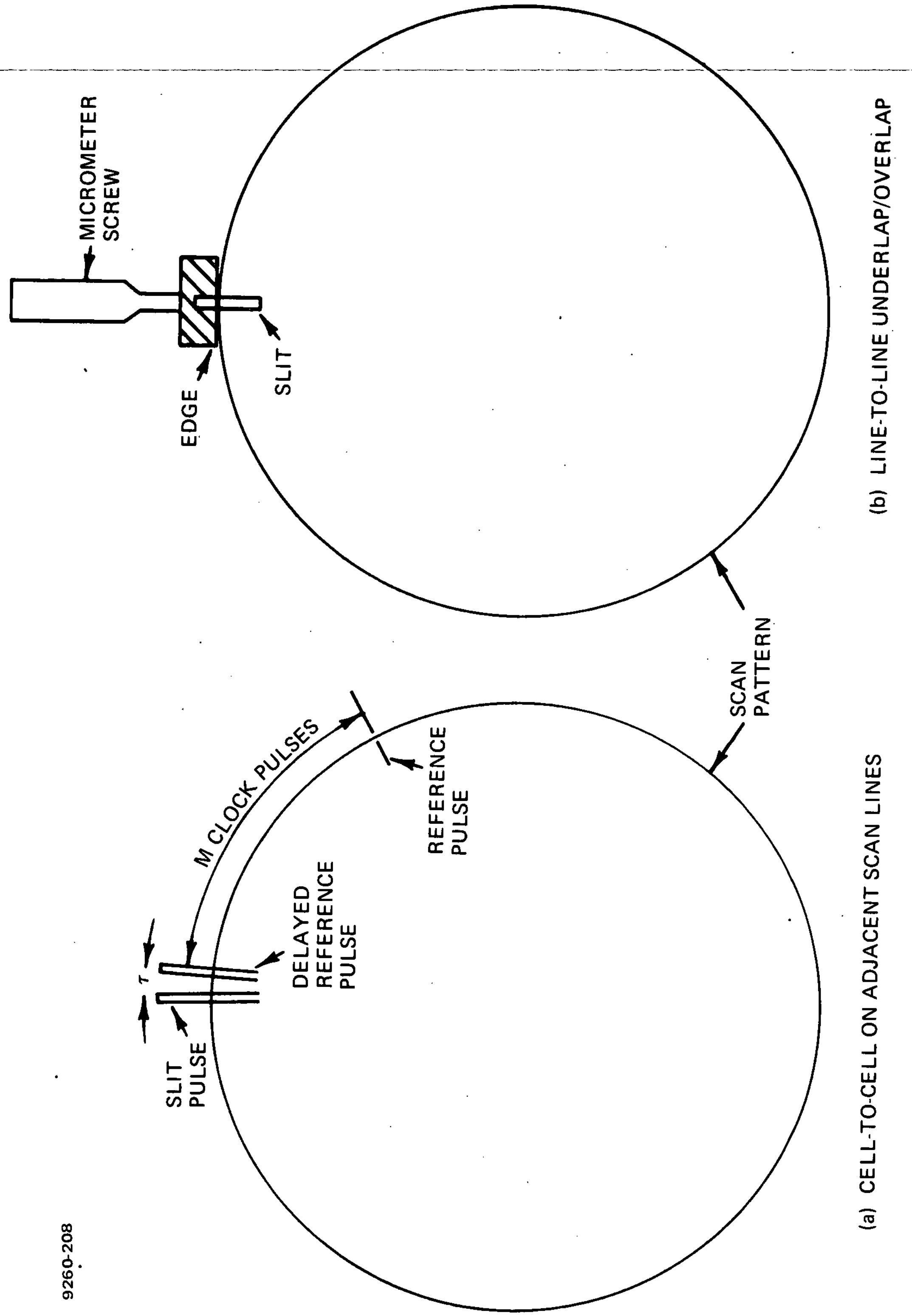

Figure 3-6 Optical Measurements of Registration Errors

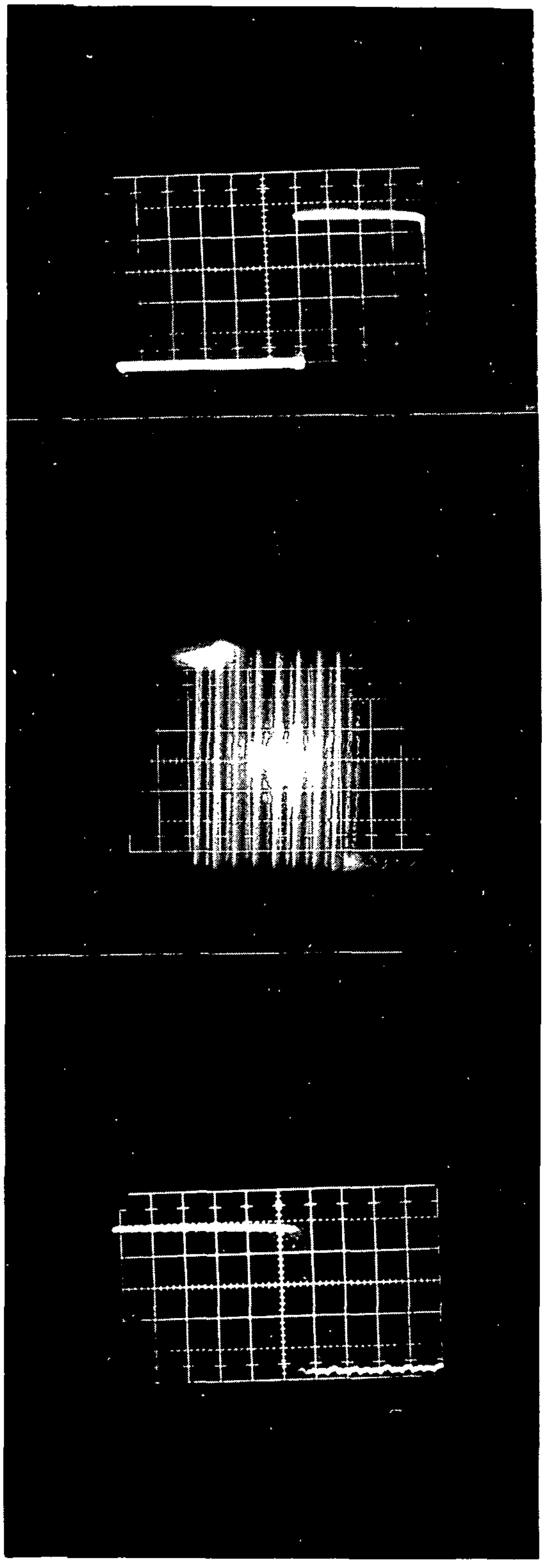

(A) SYSTEM TEST SIGNAL
VERTICAL SCALE: 1 DIV = 1 V
HORIZONTAL SCALE: 1 DIV = 1 μSEC
EXPOSURE = 1/25 SEC

(B) SYSTEM TEST SIGNAL TRAILING EDGE
VERTICAL SCALE: 1 DIV = 0.5 V
HORIZONTAL SCALE: 1 DIV = 50 NSEC
EXPOSURE: 1 SEC

(C) SINGLE ENCODER PULSE TRAILING EDGE
VERTICAL SCALE: 1 DIV = 1 V
HORIZONTAL SCALE: 1 DIV = 100 NSEC
EXPOSURE: 6 SEC

9260-209

Figure 3-7 Unloaded Test Results (Motor Speed = 1024 rpm, IFOV = 5.2 μsec) on the leading edge of the pulse, and so, the jitter which is apparent on the trailing edge is an indication of the positional accuracy of the motor shaft relative to the driving frequency. Figure 3-7(b) is an expanded view of the system test signal's trailing edge with a major division on the horizontal scale corresponding to 50 nsec. It is seen that the variation in time of the trailing edge is less than 350 nsec, or 6.7% of an IFOV element, which corresponds to 7.7 arc-sec of motor shaft rotation. However, this measurement includes both speed fluctuations and encoder jitter.

Encoder jitter is removed by dividing the system test frequency by 1800, Section 3.2.1, the number of bars on the encoder. The resulting one pulse per revolution is shown in Figure 3-7(c) and gives a direct indication of motor speed variations. It is seen that the time variation of the trailing edge is less than 100 nsec, or 1.9% of an IFOV element, which corresponds to 2.2 arc-sec of motor shaft rotation.

3.3.2 Rotor Under Load

Mounting the rotor on the motor shaft initially caused an instability in the control circuitry. Variation of the parameters comprising the motor stabilization circuitry, including the gain, corrected the situation. The resulting system test signal is shown in Figure 3-8(a). It should be noted that the change in gain has decreased the width of the pulse.

Figure 3-8(b) is an expanded view of the system test signal's trailing edge with a major division on the horizontal scale corresponding to 50 nsec. It is seen that the variation in time of the trailing edge is less than 400 nsec, or 7.7% of an IFOV element, which corresponds to 8.9 arc-sec of rotation of the motor shaft.

Again, the test described in Section 3.2.1 was performed. The results are shown in Figure 3-8(c). It is seen that the time variation of the trailing edge is less than 250 nsec, or 4.8% of an IFOV element, which corresponds to 5.5 arc-sec of motor shaft rotation.

3.3.3 Optical Test

The results of the optical test described in Section 3.2 are shown in Figure 3-9 and include both scan control errors and bearing runout. In Figure 3-9(a), the oscilloscope is triggered precisely once per revolution by the motor reference frequency divided by the number of bars on the encoder (1800). The position of the test slit pulse is then observed referenced to the system crystal oscillator. Cell-to-cell registration on adjacent scan lines is measured as variations in this position and is represented in Figure 3-9(a) by the thickness of the line. It is seen that the line thickness is approximately 450 nsec, which

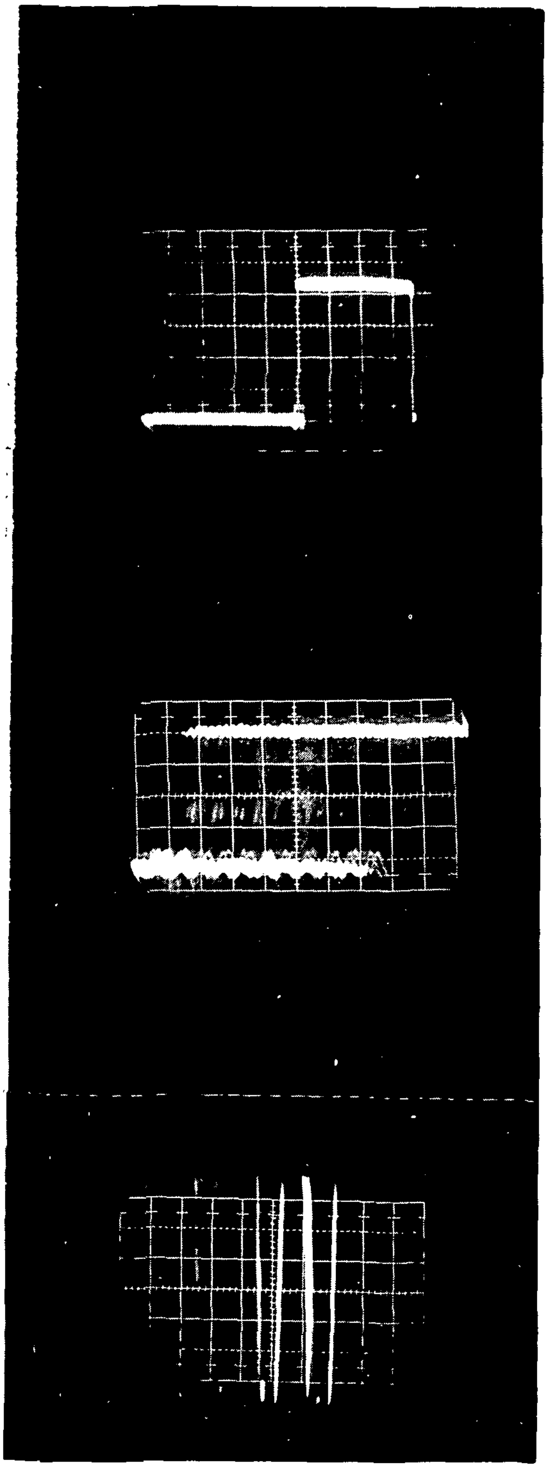

(A) SYSTEM TEST SIGNAL
VERTICAL SCALE: 1 DIV = 1 V
HORIZONTAL SCALE: 1 DIV = 1 μSEC
EXPOSURE: 1/25 SEC

(B) SYSTEM TEST SIGNAL TRAILING EDGE
VERTICAL SCALE: 1 DIV = 1 V
HORIZONTAL SCALE: 1 DIV = 50 NSEC
EXPOSURE: 1 SEC

(C) SINGLE ENCODER PULSE TRAILING EDGE
VERTICAL SCALE: 1 DIV = 0.5 V
HORIZONTAL SCALE: 1 DIV = 50 NSEC
EXPOSURE: 5 SEC

Figure 3-8 Loaded Test Results From the Encoder
(Motor Speed = 1024 rpm, IFOV = 5.2 μsec)

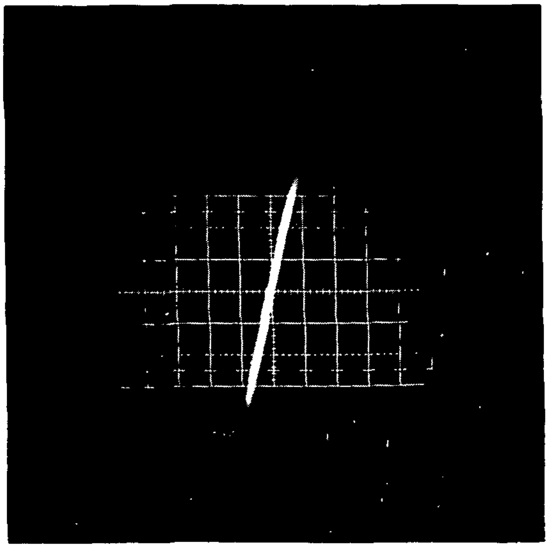

(A) CELL-TO-CELL REGISTRATION ERROR,
HORIZONTAL SCALE: 1 DIV = 1 μSEC

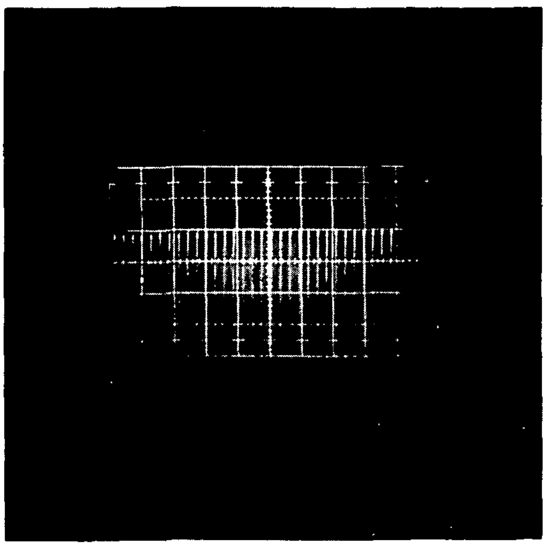

(B) LINE-TO-LINE UNDERLAP/OVERLAP,
VERTICAL SCALE: 3.2 DIV = 1 IFOV

9260-211

Figure 3-9 Optical Test Results

corresponds to a cell-to-cell registration error of 8.7% of one IFOV element, or 10.2 arc-sec of rotation on the circle scanned by the rotor arm.

Line-to-line underlap/overlap errors are shown in Figure 3-9(b). In this figure, 3.2 divisions correspond to one IFOV element and the height of each pulse is proportional to line-to-line registration errors. It is estimated that the pulses are the same height to within 5% of one IFOV element.

3.3.4 Comparison With Expected Values

In Section 4.5.3, Volume I, of the OSS Final Report, it was determined that the accuracy achievable with the scan control electronics is 2.0 arc-sec compared with the field of view which corresponds to 115 arc-sec of rotation. One of the components used in this calculation is the encoder line density—assumed to be 6480 lines per revolution. In the breadboard motor, however, the encoder has only 1800 lines per revolution—which would give an achievable accuracy of 7.2 arc-sec. In Section 3.3.2, it was shown that the scan control electronics is capable of 5.5 arc-sec positional accuracy. A further calculation was made in Section 4.5.3 (Vol I)—that of the over-all positional accuracy achievable with the scan control. If an encoder density of 1800 lines is substituted for the 6480-line encoder assumed there, the over-all accuracy would be 7.6 arc-sec. This figure, it should be noted, still assumes that a state-of-the-art encoder is used (see Section 3.1.2). The results obtained in breadboard tests have indicated that an over-all scan control positional accuracy of 8.9 arc-sec is achievable. This figure would improve if a more sophisticated encoder were incorporated in the breadboard motor.

When bearing runout is taken into account, the positional accuracy measured on the breadboard reduces to 10.2 arc-sec. Under the assumption that both scan control errors and bearing runout are random and independent of one another, bearing runout causes up to 5 arc-sec of positional inaccuracy. As discussed in Section 4 of Vol 1, a more sophisticated bearing arrangement would be used in a flight unit and should reduce these errors to about 3 arc-seconds of positional accuracy. This would also apply to line-to-line underlap/overlap registration errors which, in a flight unit, should be reduced to about 3% of one IFOV element.

SECTION 4

ELECTRONICS BREADBOARD

Two channels of electronics have been designed, fabricated, and tested as part of the Bendix-sponsored activities carried out in conjunction with the OSS study contract. Each channel consists of an analog processor, A/D converter, and buffer; the performance of these stages is described in the following sections. In addition to constructing these stages, it is necessary to supply the timing and control information required for their correct operation. The appropriate logic circuitry has therefore been constructed and provides the scan start frequency, correct timing for the integrate-hold-dump cycle, A/D conversion times, calibration periods, and the read/write timing required for the buffer. This logic and the electronics breadboard are built into the console shown in Figure 4-1, which also contains the logic for the motor control and registration tests discussed in Section 3.

4.1 ANALOG PROCESSOR

The analog processor, Figure 4-2, performs the functions of additional gain, gain control, dc offset, plus integration and sampling of the signal. Of the three cards shown in Figure 4-2, the first contains the amplification, integration, and sampling circuitry; the center card contains level shifters which provide the appropriate voltages for the analog switches used in the analog processor; and the third card provides the dc offset and gain control circuitry. As described in Section 9 of Vol I, the gain and offset are dependent on the high and low calibration source levels. In a flight model, these levels would be selected on command by switching different filters in front of the calibration sources. However, the calibration source levels are electrically simulated on the breadboard. During each scan period, four calibration sources are viewed which are in turn: (1) low-temperature blackbody, (2) visible high calibration, (3) visible low calibration, and (4) high-temperature blackbody. These four calibration levels will always appear as constant voltage levels at the analog processor output as shown in Figure 4-3(a) which shows the response of the analog processor (gain ≈100) to a low frequency sine wave. The sampling frequency is relatively high so that its effects are only noticeable as a slight broadening of the trace corresponding to the period for which the sampled value is held. The active portion of each scan period is from the start of the trace to just before the first calibration level. Figure 4-3(b) shows the response of the analog processor to a frequency of about 16 kHz on which the

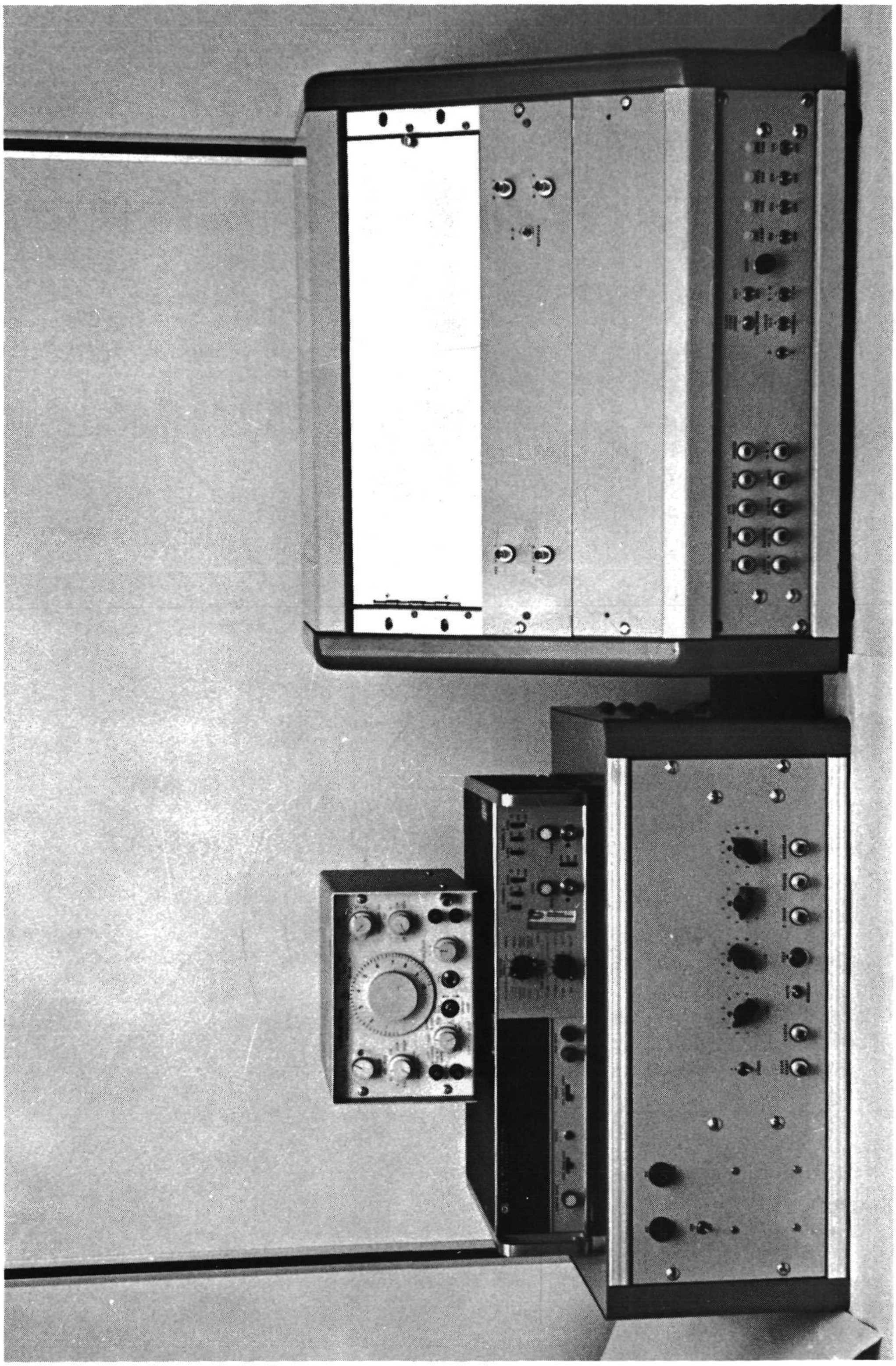

9260-212

Figure 4-1 Photograph of the Electronics Breadboard Console

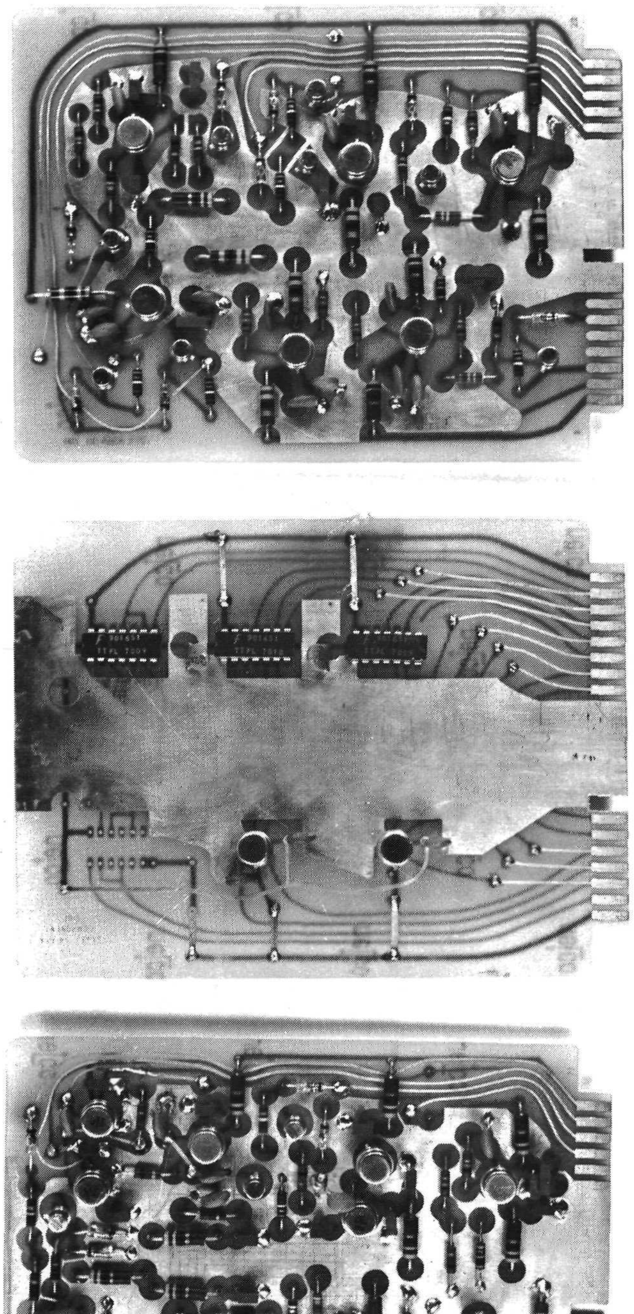

9260-213

22182

Figure 4-2 Photograph of the Analog Processor Cards

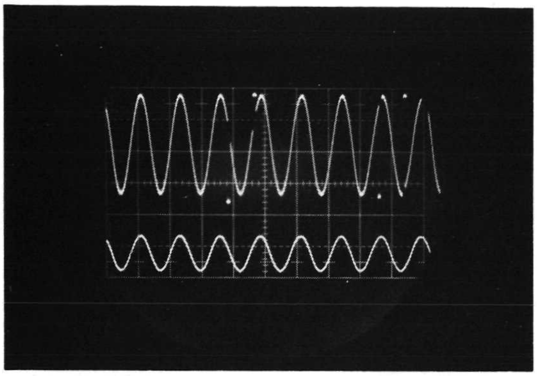

(A) 140 Hz SHOWING FULL SCAN PERIOD AND CALIBRATION LEVELS
(Low to High Cal ≈ 4.5V)

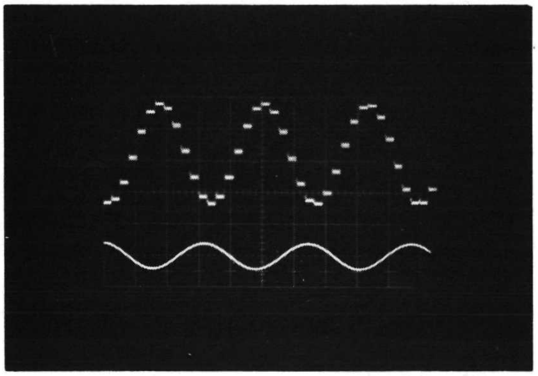

9260-214

(B) 16 kHz SHOWING SAMPLED OUTPUT

Figure 4-3 Response of the Analog Processor (Upper Trace to a Sinewave Input (Lower Trace) sampled values can clearly be seen. The sampling frequency is 192 kHz and A/D conversion of the signal takes place while the signal is held, well away from switching transients. The trace shows an apparent thickness to the held signal levels which arises since the input frequency is not an exact division of the sampling frequency. The sampling frequency therefore drifts relative to the signal during the exposure of the photograph. If a single-trace photograph could be recorded, the sampled values would appear much narrower.

The frequency response of the analog processor is illustrated in the traces shown in Figures 4-4(a) through 4-4(c). In these figures, the input is a continuous sweep of the frequency. Thus, Figure 4-4(a) shows the low-frequency response from 300 Hz up to approximately 30 kHz, while Figure 4-4(b) shows the frequency response from 30 kHz out to just beyond the first zero in the MTF of the integrator which occurs at 240 kHz. Figure 4-4(c) shows the high-frequency response with the frequency sweep starting at about 100 kHz and extending to beyond 700 kHz. The successive minima in the high-frequency response can readily be seen, and they give the MTF a form which has a noise bandwidth which is considerably less than that for a Butterworth filter with the same 3-dB cutoff frequency. Measurements of the analog processor response to a continuous sine wave input show that it is 3 dB down at about 100 kHz. The effects of sampling can clearly be seen as striations in Figure 4-4, particularly at frequencies which are an exact division of the sampling rate.

4.2 A/D CONVERTER

During the design study, two A/D converters were evaluated, with close regard to the low power requirements. Assuming continuous operation, the selected A/D converter requires 270 mW of power. As discussed in Section 9, Vol I, there are a total of 38 A/D converters (1 per channel) and they consume a total power of 10 1/4 W. Figure 4-5 is a photograph of the breadboard A/D converter, and Figure 4-6 shows its output (lower trace) after passing through a D/A converter. The upper trace is the input sine wave to the analog processor. The apparent broadening of the sine wave output is largely due to the period for which the sampled values are held.

4.3 BUFFER

Both the plated wire memory and the newer MOS dynamic shift register have been evaluated. The latter was selected for the OSS Scanner since its performance is adequate for this application and it requires considerably less space, weight, and power than does the plated wire memory. An MOS buffer would result in savings of 20 lb of weight and 9 W of power for the scanner over a plated wire memory. Figure 4-7 is a photograph of the buffer; the lower trace of Figure 4-8

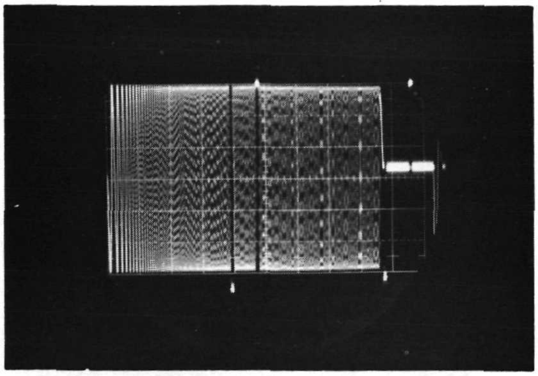

(A) 300-Hz TO 30-kHz SWEEP

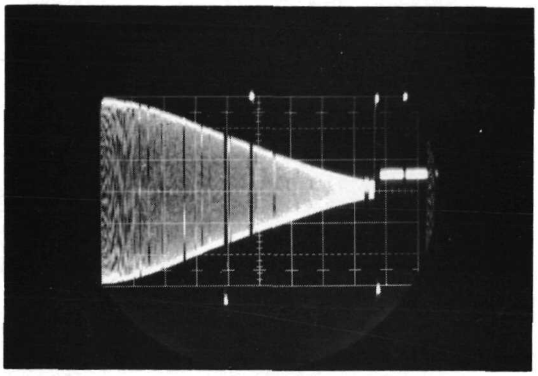

(B) 30-kHz TO 250-kHz SWEEP

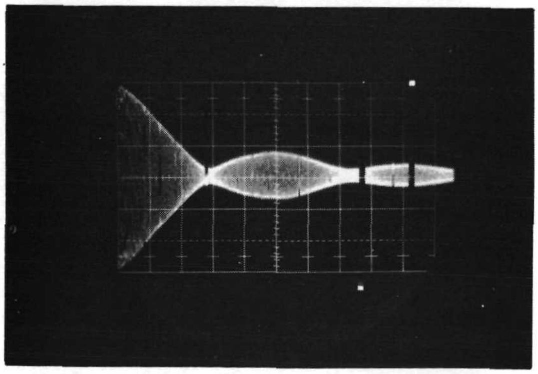

9260-215

(C) 100-kHz TO 700-kHz SWEEP

Figure 4-4 Frequency Response of the Analog Processor

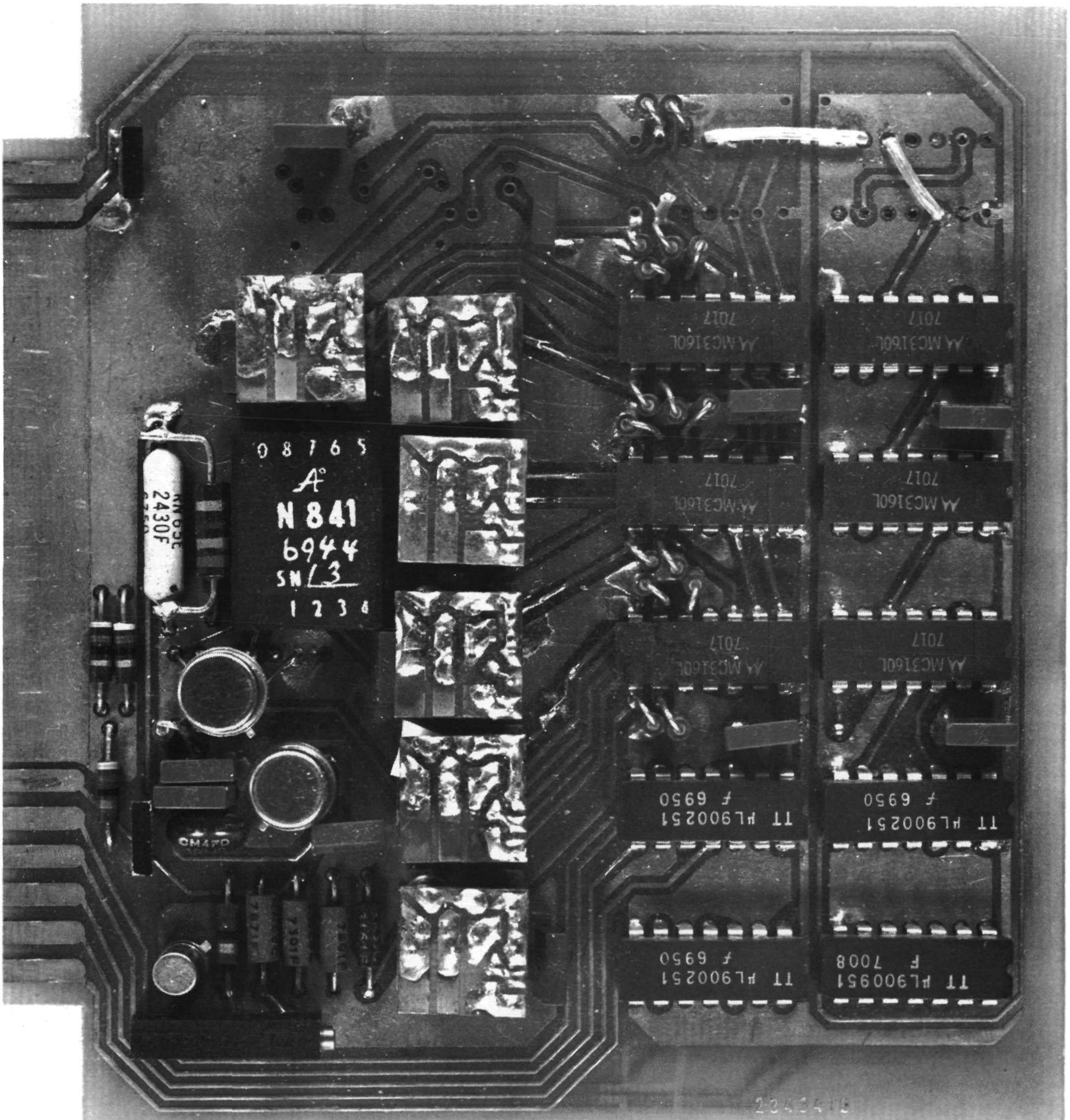

9260-216

22180

Figure 4-5 Photograph of the A/D Converter

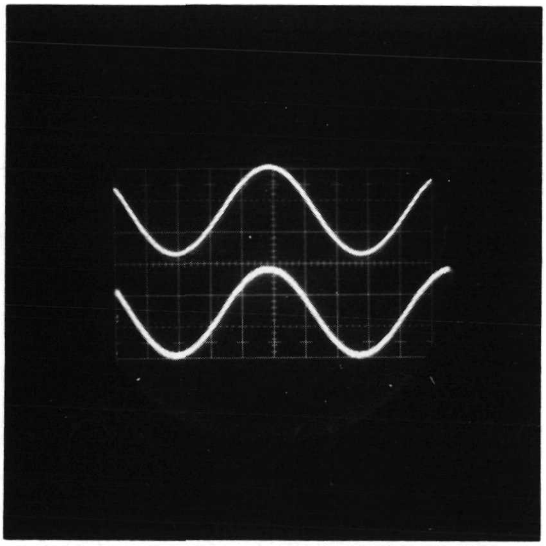

9260-217

Figure 4-6 Upper Trace: 1.6 kHz Input to Analog Processor (0.015 V/cm)
Lower Trace: A/D Converter Output Seen Through D/A Converter (1.5 V/cm)

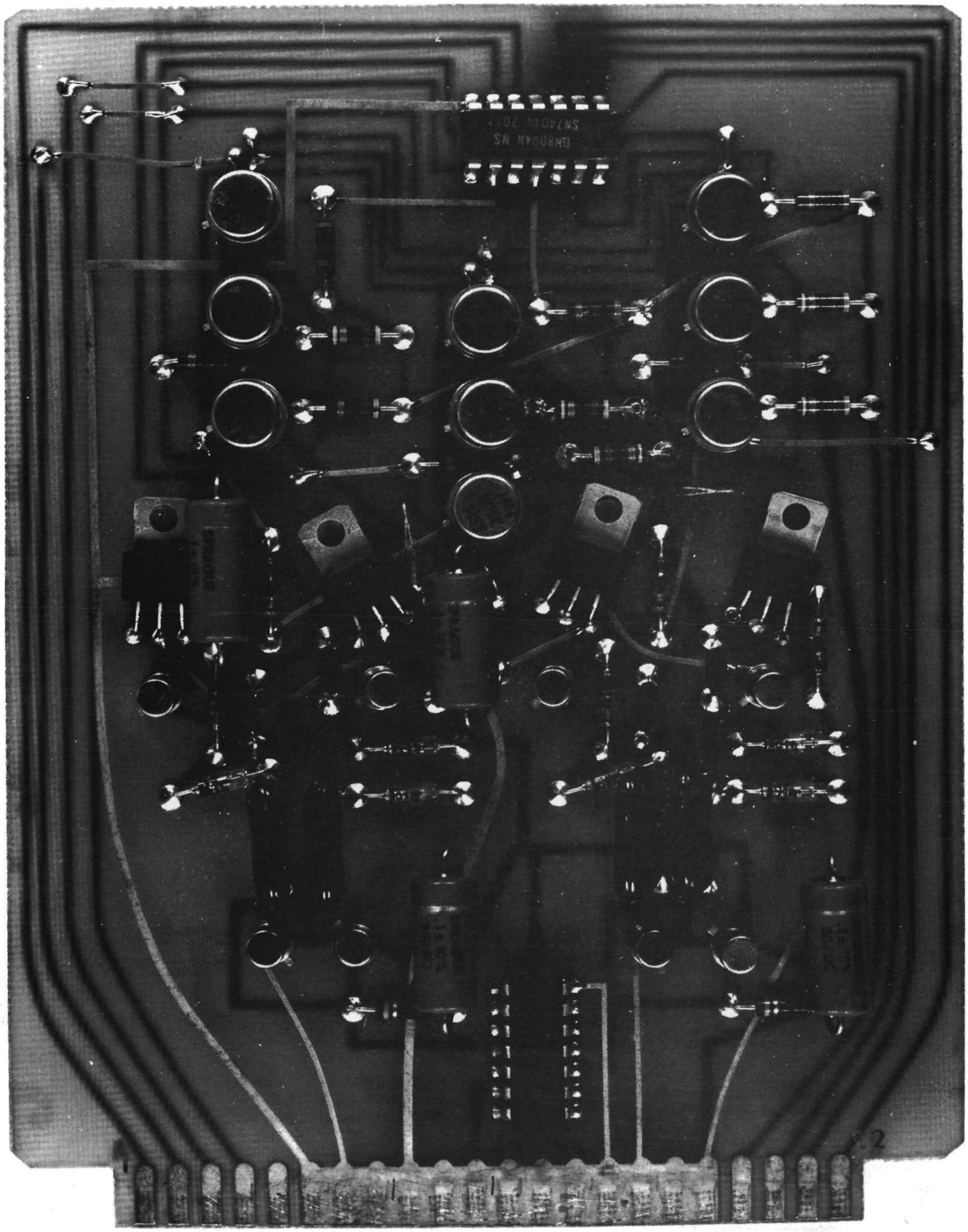

Figure 4-7 Photograph of the MOS Buffer

9260-218

22181

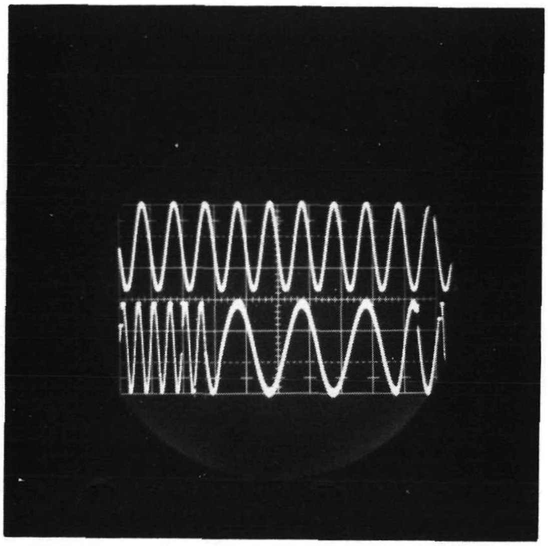

9260-219

Figure 4-8 Upper Trace: Input to Analog Processor (0.015 V/cm)
Lower Trace: Buffer Output Observed Through a D/A Converter (1.5 V/cm)

shows its output observed after passing through a D/A converter. The upper trace is the input to the analog processor. When observed through the whole system, it is seen that the input signal is compressed by a factor of two for the active scan period and expanded by a factor of two for the rest of the scan period. Only this second part of the trace is pertinent to the OSS Scanner, since the buffer output would be gated to transmit stored data only during the nonactive data taking period. The data which are transmitted during the active scan period are transmitted in real time and do not pass through the buffer. The buffer output during the non-active scan period is one-half of the signal frequency, since data are read out of the buffer at one-half the input data rate to the buffer. For purely academic interest, the frequency is doubled during the active scan period since these data (in practice not transmitted) are read into the buffer during the nonactive scan period. It is therefore read out during the active scan period at twice its input rate.

SECTION 5

DOUBLE-DUTY CYCLE TECHNIQUES

Although a conical scan line, produced by an object plane scanner as well as by an image plane scanner, corresponds to a relatively high duty cycle compared with a linear scan line, there is a reasonable desire for a further increase of the duty cycle. This would further increase the sensitivity while easing electronic design requirements and decreasing the buffer size, power, and weight.

One way to achieve a higher duty cycle is to construct a scan mechanism which is able to write more than one scan line per motor revolution. Since this results in an increase in the number of scan mirrors corresponding to the number of scan lines, serious problems are immediately encountered with an object plane scanner because of the size of the scan mirror. The advantage of the image plane scanner, however, is just the small size of the scan mechanism. Thus, the attempt to modify this mechanism in order to increase the duty cycle suggests itself. In any case, increasing the number of scan mirrors greatly increases the alignment problems since the mirrors must be very precisely aligned relative to one another. If they are not, registration errors will be correspondingly increased.

Three different methods of doubling the duty cycle are discussed in the following subsections. The components of the scan mechanism are essentially the same for all three methods, Figure 5-1, and consist of a wedge-shaped center mirror and two outer mirrors in diametrically opposite positions. In one case, the doubling is caused mechanically, in the other cases by different optical arrangements.

5.1 TRANSLATING CENTER MIRROR

A theoretically elegant, but in practice a little complex, solution of this problem is to superimpose a translatory motion to the rotating center mirror during the nondata taking period so that a reflecting surface of the center mirror is on axis and facing the second scan mirror whenever a data taking period becomes due.

A mechanical concept of this technique is illustrated in Figure 5-2. The end of the drive shaft is square so that it will fit within a longitudinal hole in the central mirror wedge, which permits a lateral motion during the rotation. The movement is controlled by a cam roller moving within the guide receptacle. This receptacle

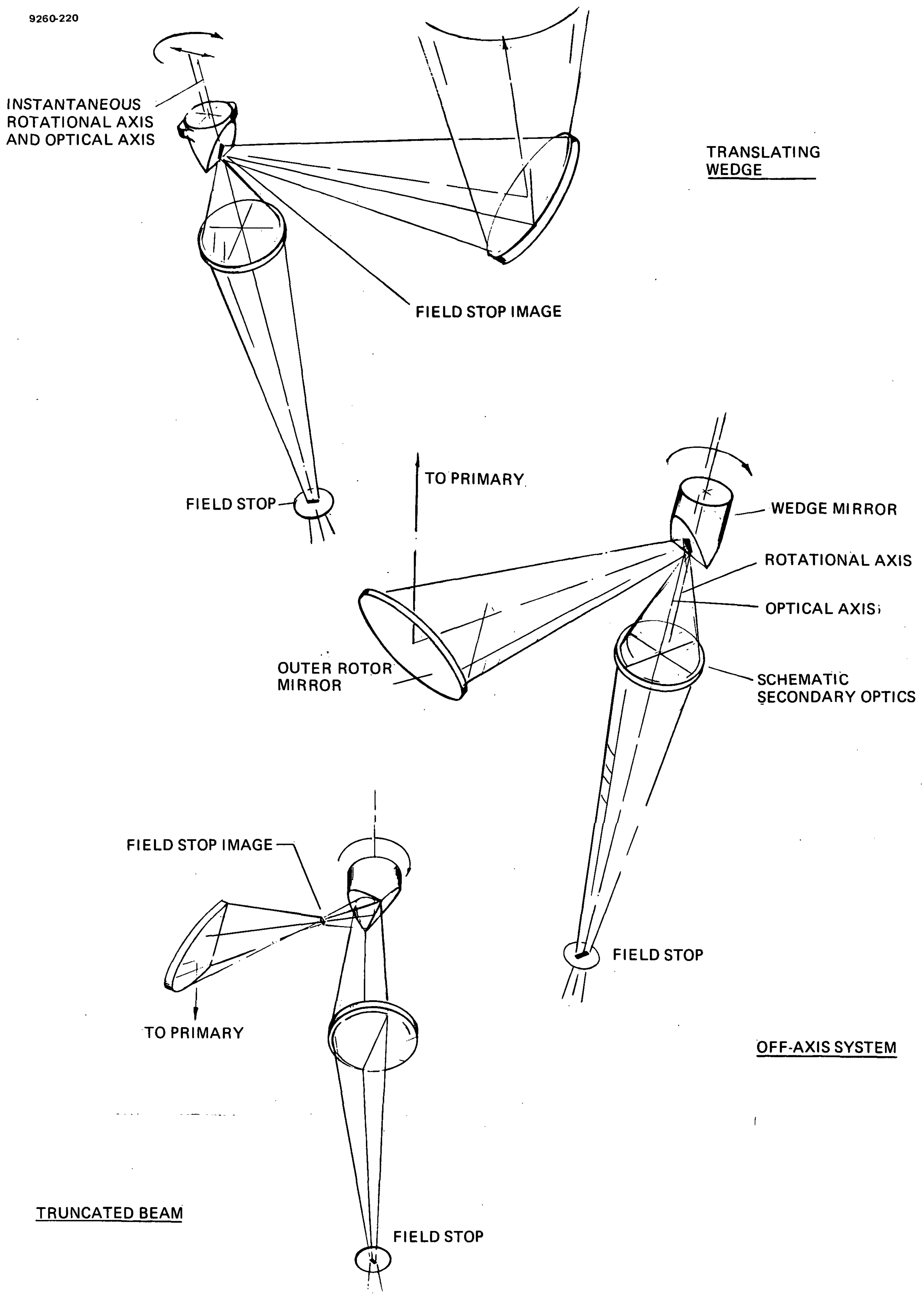

Figure 5-1 Alternative Methods for Doubling the Duty Cycle

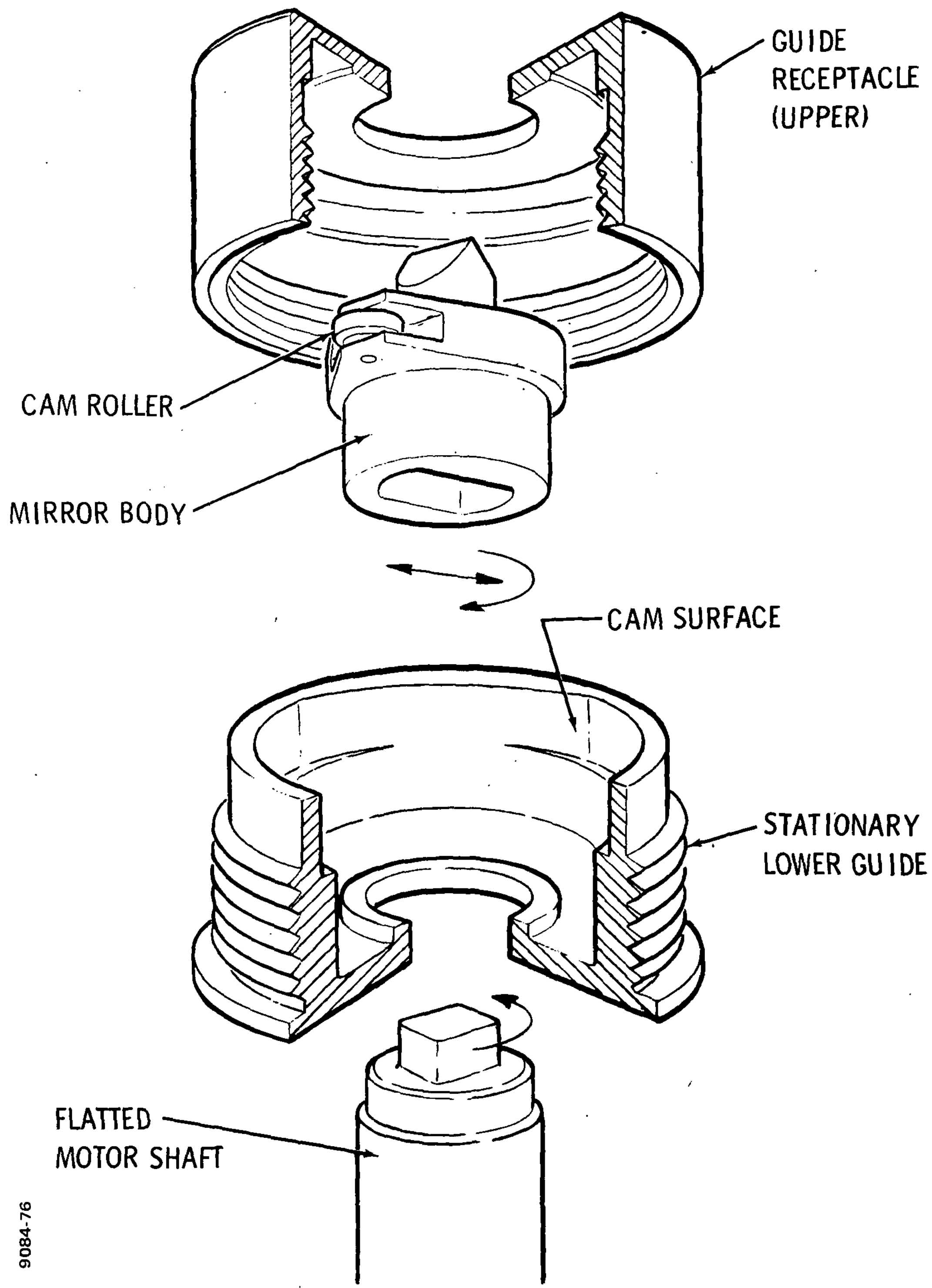

Figure 5-2 Mechanical Concept for Translating the Central Mirror

is machined to a very precise shape, which ensures that the central wedge moves by the correct amount during the rotation. To keep the translation of the center mirror as small as possible, it is necessary to have the crossover right on its surface. In this case, the total amount of the translation is determined by the image of the field stop, taking into account the blur circle caused by the spherical aberration of the primary. The size of the field stop corresponding to one resolution element is 0.084 mm x 0.084 mm. The secondary produces a demagnification of a factor 2.5 which makes an idealized image size of 0.021 mm x 0.021 mm. The blur circle of the primary, however, has a diameter of 0.68 mm, and since the field stop is a slit corresponding to six elements of resolution, the total amount of translation according to Figure 5-3 is 0.8 mm. The relationship between the positioning tolerance of the central wedge, S, and the angular registration error γ in object space is given by:

$$\Delta_1 = \Delta_2 = S = \gamma \cdot F_1$$

where

Δ_1 = misregistration

Δ_2 = defocusing

F_1 = 50.8 cm = focal length of the primary.

If γ is to be a tenth of the IFOV (6.6 μrad), then

$$\Delta_1 = \Delta_2 = 3.4\ \mu m$$

The guide receptacle and cam roller must therefore be so machined that the motion imparted to the wedge does not depart from the ideal motion by more than 3.4 μm (or 0.00013 in.). It is doubtful if this tolerance can be met in practice, and translating the central wedge is therefore not considered a viable technique for increasing the duty cycle.

5.2 OFF-AXIS SCANNING

The second way to achieve a double-duty cycle has to put up with the fact that mostly during a data taking period the primary optics work slightly off axis. The optical arrangement is such that both the image of the field stop and the focus of the primary exactly coincide on the surface of the wedge when the position of the rotor corresponds to the center of a scan line. This is the only instant when the complete system works on axis. At any different position, the secondary is imaging an element of area which is off axis and defocused with respect to the primary.

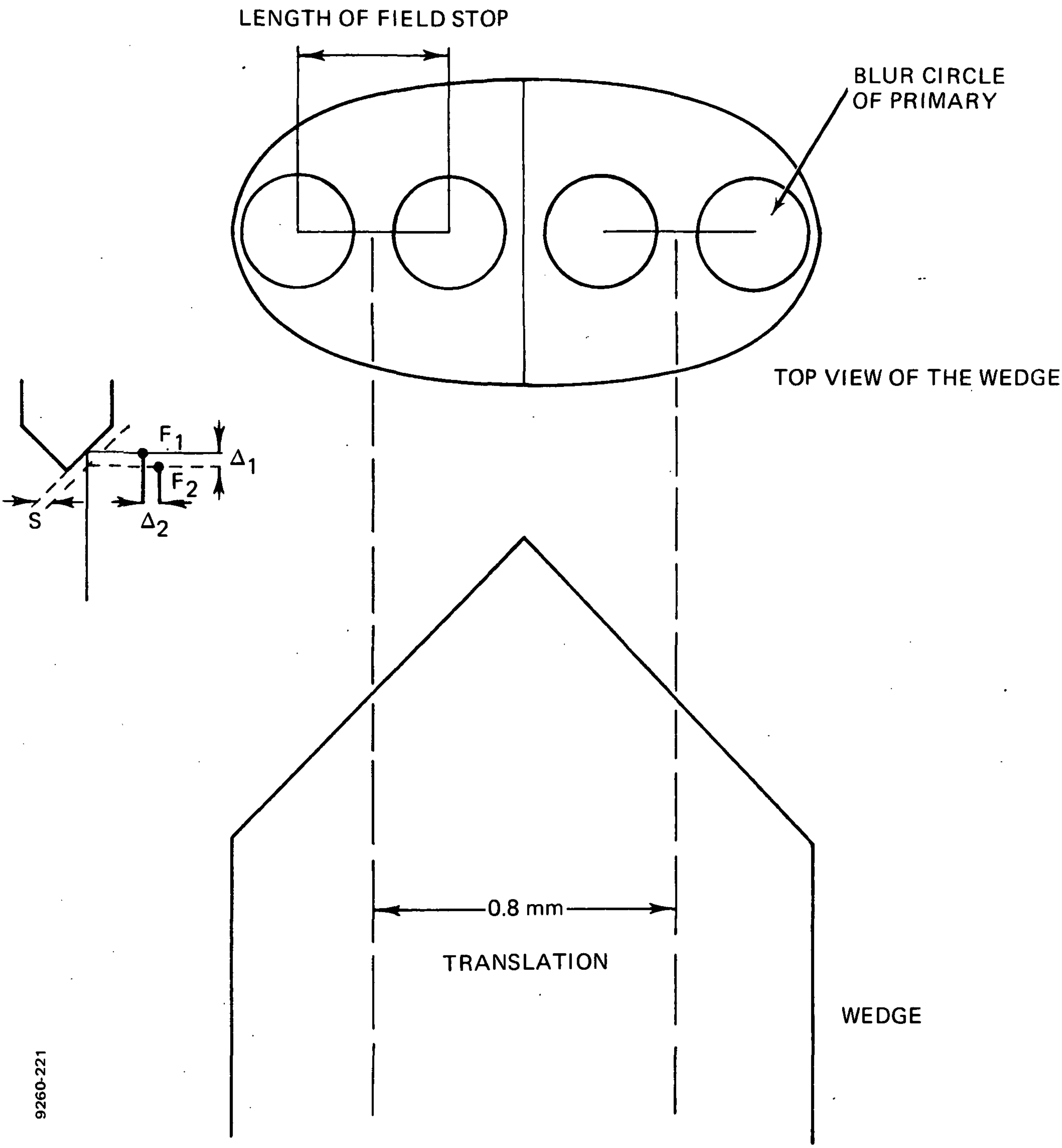

Figure 5-3 Translating Center Mirror

According to Figure 5-4, the relation between the scan angle ϕ and the defocusing Δ_1, or the off-axis distance Δ_2, is given by:

$$\Delta_1 = r(1 - \cos\phi)$$

$$\Delta_2 = \sqrt{\Delta_2'^2 + \Delta_2''^2}$$

where

$$\Delta_2' = r(1 - \cos\phi)$$

and

$$\Delta_2'' = r \cdot \sin\phi$$

The parameter r is the distance between the image of the field stop and the center of the wedge at the central scan position.

Another consequence of this technique to double the duty cycle is that the scan line is no longer an exact circle but a curve given by the parametric representation:

$$x = \sqrt{R^2 + 2r(R + r)(1 - \cos\phi)} \cdot \cos\phi$$

$$y = \sqrt{R^2 + 2r(R + r)(1 - \cos\phi)} \cdot \sin\phi$$

where R is the radius of scanning circle in the focal plane of the primary and r is the above-mentioned distance of the image of the field stop from the center of the wedge. Since $r \ll R$, the equations may be simplified to:

$$x = R \cdot \sqrt{1 + \xi(\phi)} \cdot \cos\phi$$

$$y = R \cdot \sqrt{1 + \xi(\phi)} \cdot \sin\phi$$

wherein $\xi(\phi) = 2r/R \cdot (1 - \cos\phi)$ gives the deviation from a true circle.

To obtain numerical values for Δ_1 and Δ_2, it is necessary to calculate r. This is determined by the extent of the aberrated image of a cell formed by the primary and the semiscan angle of 60°. From Figure 5-4, it is seen that

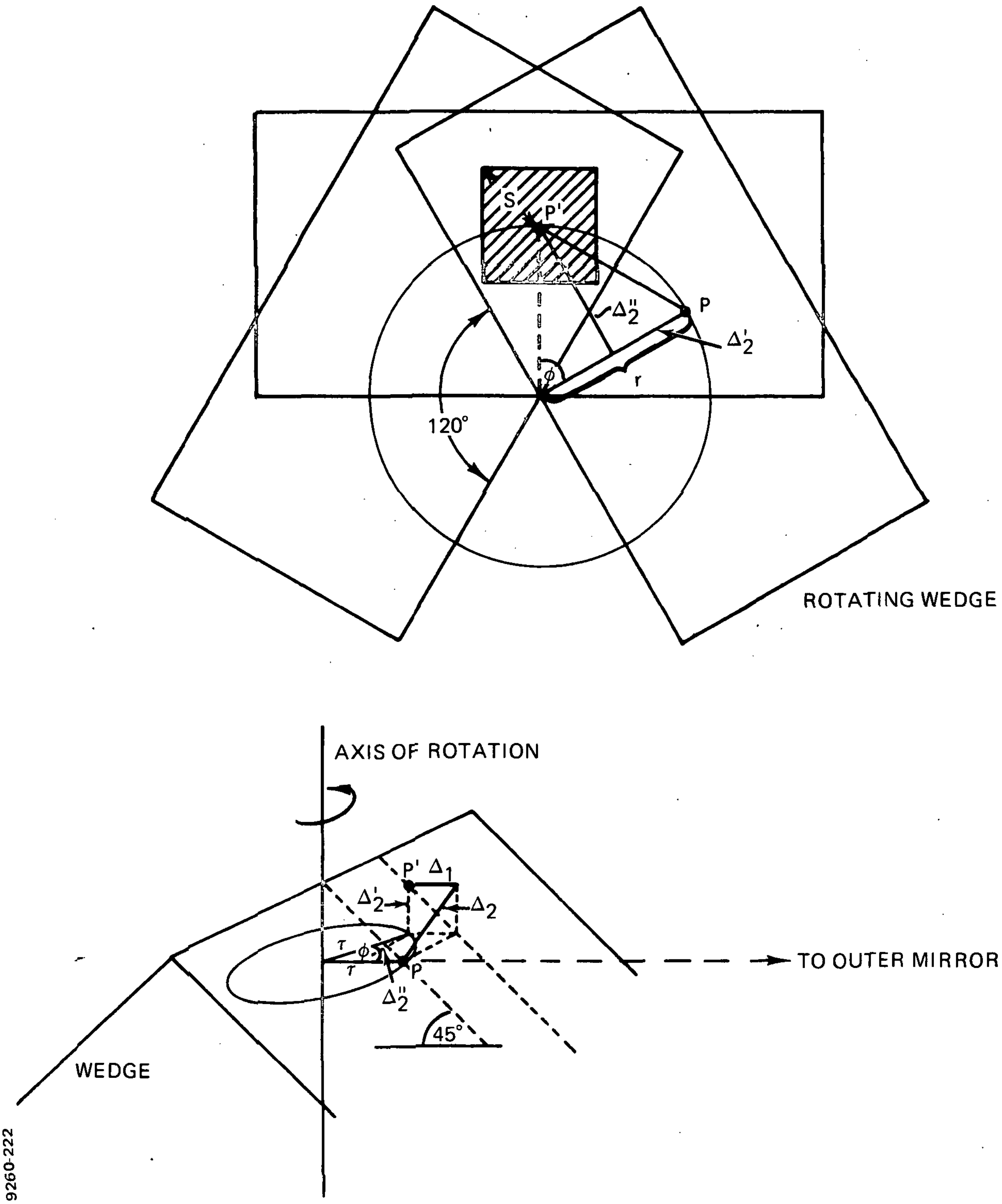

Figure 5-4 Off-Axis Scanning

$r \simeq s/\cos 60° = 2s$ where s is the semidiagonal of one resolution element plus the radius of the blur circle produced by the primary. Using the values given in Section 5.1, one gets:

$$s = (0.01 \cdot \sqrt{2} + 0.34) \text{ mm} = 0.35 \text{ mm}$$

so that

$$r = 0.7 \text{ mm}$$

The maximum Δ values therefore are:

Defocus: $\Delta_1 = 0.35$ mm

Off axis: $\Delta_2' = 0.35 \text{ mm} \hat{=} 0.7$ mrad

$\Delta_2'' = 0.61 \text{ mm} \hat{=} 1.2$ mrad

which is about a factor of 10 higher than allowed for a system having the required resolution of 0.066 mrad. This approach to doubling the duty cycle is therefore also not viable.

5.3 TRUNCATED BEAM

The third method to achieve a doubling of the duty cycle may seem to be a little radical, but because of its simplicity and because of the fact that the optical performance essentially does not differ from what was found for the single-duty cycle system, it turned out to be the most promising one. If the rotor is thought of as applied for a single duty cycle, and the center mirror is cut so that a symmetric wedge with its edge right through the axis of rotation is obtained, one realizes that the cross section of the beam then will no longer be a full circle but a semi-circle. By turning over the central wedge so that the beam is reflected back to the primary, an arrangement is obtained where only the outer portion of the primary is used, Figure 5-5. The advantage of this configuration is that it gives space for placing the secondary system at the center of the primary mirror, which makes the entire optical system optimally compact.

However, it should be noted that nearly all the obscurations which arise in the single scan arm version (31% duty cycle) do not arise in the truncated beam method of doubling the duty cycle. This is because the obscuration principally occurs in the half of the beam which is cut away to achieve the doubling. The loss

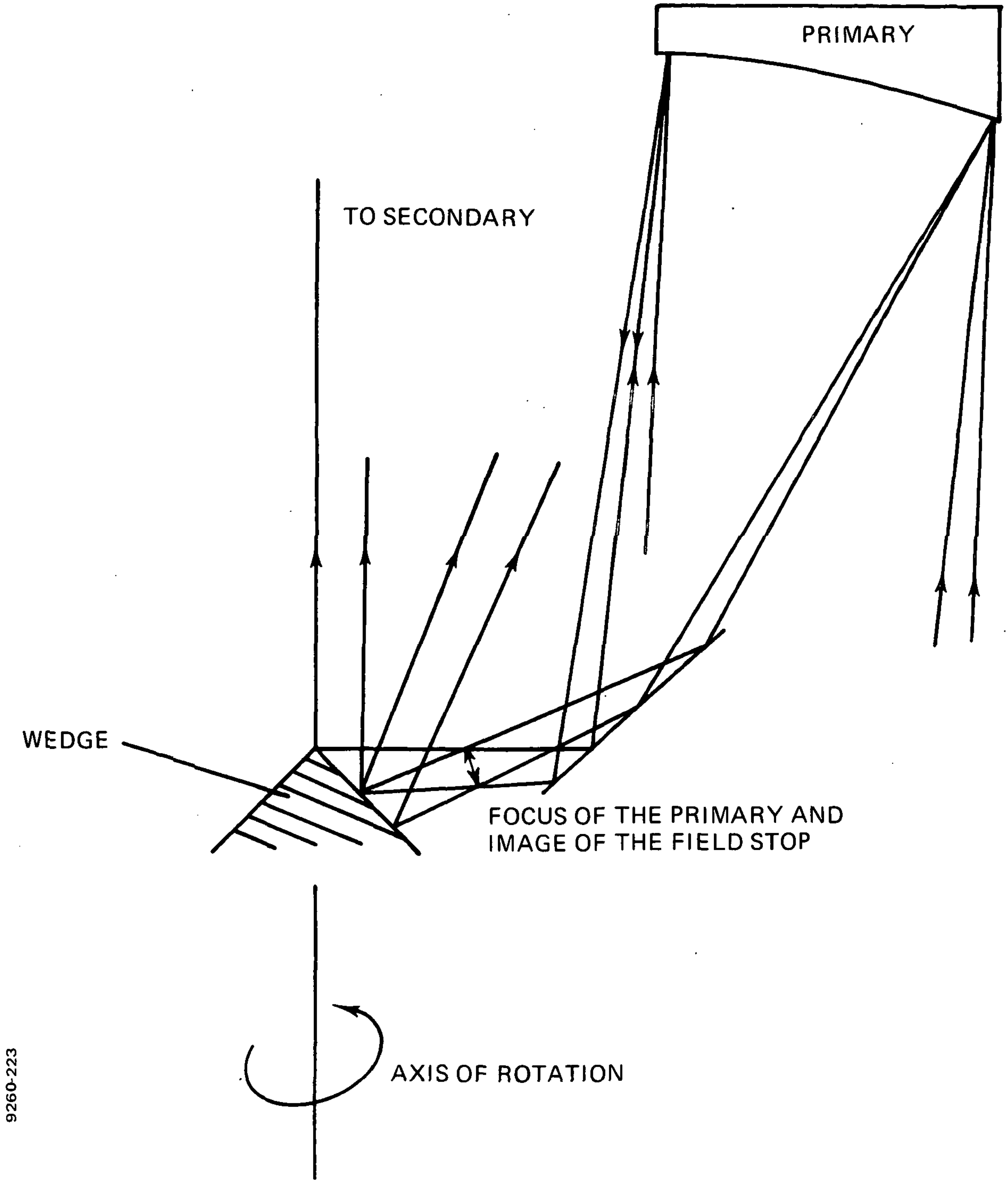

Figure 5-5 Truncated Beam

in energy is therefore only some 25% and not 50%, resulting in a smaller increase to the size of the primary than would be expected at first sight if the same quantity of energy is to be collected as with the single scan arm. The compact nature of the optical arrangement can be envisaged from Figure 5-6 which shows how the secondary mirror can be situated so as to cause no obscuration to the primary aperture.

This last technique for doubling the duty cycle is the most practical of the three alternatives discussed. It remains only to note that the two outer mirrors and the central wedge should be aligned (relative to one another) to angular tolerances of less than 10 arc-sec and separations of 3.4 μm (0.00013 in.) in order to maintain registration to within 10% of one IFOV element. These tolerances arise directly from the equations given in Section 3.4 of Vol I. It would be difficult to machine the rotor arm to this kind of accuracy, and both outer mirrors must therefore have precision adjustments. The central wedge can be optically worked to the required accuracy and would not have to be adjustable.

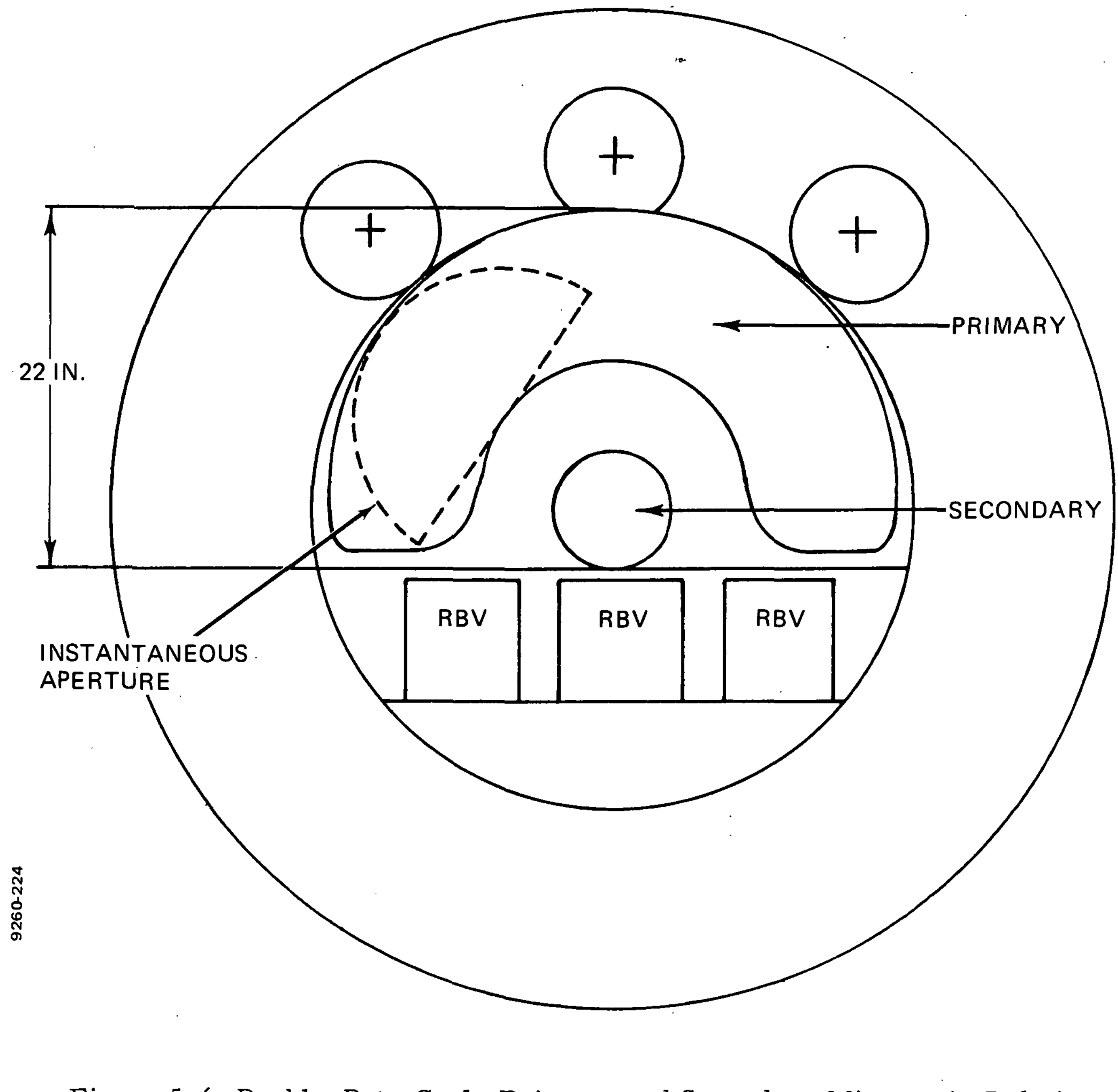

Figure 5-6 Double-Duty Cycle Primary and Secondary Mirrors in Relation to the ERTS Spacecraft Torus

5.4 SUMMARY

Having selected the truncated beam technique as the most applicable method for increasing the duty cycle, a brief investigation was made of the resulting increase in sensitivity which can be expected for the ERTS spacecraft envelope. Apart from showing the compact nature of the double-duty cycle technique, Figure 5-6 shows the size of the primary mirror which could be incorporated into the available envelope. The scanner would look directly downward, thus fitting neatly in the spacecraft torus, with the spectrometers packaged directly above the secondary mirror. Figure 5-7 shows a side view of the scanner. It is seen that the secondary and scan mechanism assembly would be deployed, being folded underneath the primary mirror prior to launch. This is not considered a large drawback, since a precise, one-time operation for deploying the assembly is quite feasible.

A natural extension to doubling the duty cycle is to consider the possibility of increasing the number of arms on the rotor to three or more, thus increasing the duty cycle to over 90%. However, a tradeoff then exists between the maximum collecting area A which can be fitted into the envelope, the duty cycle δ , and system considerations such as increasing the already critical alignment tolerances. Table 5-1 provides the tradeoff between the number of arms for the ERTS envelope based on relative sensitivity. For ease of interpretation, relative sensitivity is defined here as the product $A\sqrt{\delta}$, normalized to 100 for the single-arm scan mechanism. The table shows that the diameter of a circle with the same area as the instantaneous clear aperture increases considerably for the two-arm mechanism. This is because the compact nature of the system permits use of a much larger primary mirror. The resultant increase in sensitivity is 79%. There is, however, a maximum size for the primary mirror so that as the number of arms is increased, and the aperture further truncated, the instantaneous clear aperture decreases. This decrease almost exactly compensates for the increase in sensitivity due to the higher duty cycle when the number of arms is increased from two to three. However, above three arms, the duty cycle is already near maximum while the collecting area and, hence, sensitivity decrease.

The choice between two and three arms is dependent on system considerations, particularly the increased alignment difficulties vs. the power consumed by the buffer (about 9 W for the two-arm system). It should also be noted that the selected input tape format for the GDHS (Volume 1, Section 13) could not be maintained with a three-arm system, or for any system with a duty cycle greater than 66%.

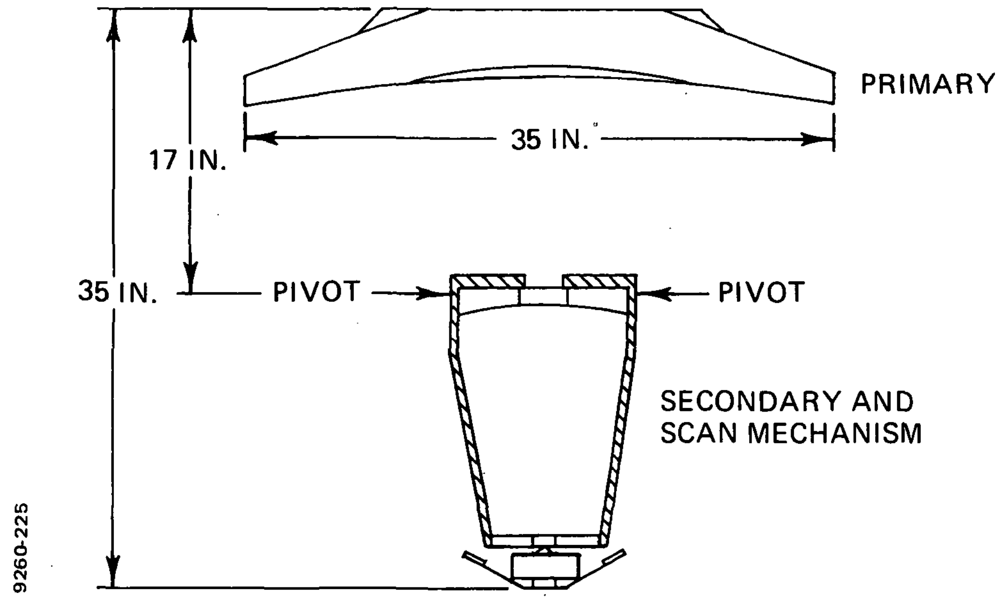

Figure 5-7 Double-Duty Cycle Primary and Secondary Mirrors in Relation to the ERTS Spacecraft Torus

TABLE 5-1

NUMBER OF ARMS VS. RELATIVE SENSITIVITY

Number of Arms	Duty Cycle (%)	Diameter of Effective Collecting Area (in.)	Relative Sensitivity
1	31.5	10.1	100
2	63	12.8	179
3	94.5	10.2	176
4	96	8.9	155